COMMERCIAL

AEEW M309

The First Core in DIMPLE at A.E.E. Winfrith - Experimental Results

by

A. G. Collins W. H. Taylor G. M. Wells

including work by

M. Singleton R. E. B. Strathen Mrs. J. M. Symes

Abstract

The results obtained during experiments on the first S.G.H.W. core in DIMPLE are presented in this report in the form of raw data. No attempt to apply theoretical corrections to allow comparison with theory has been made, since this will be included in a more general report covering a series of S.G.H.W. experiments.

The report is intended to be complete in itself, and should provide a record of all important results obtained on this core. Less essential details are recorded in the original experimental log books.

A.E.E.,
Winfrith.

August 1963.

W.5877.

Contents

1. Introduction

This report describes the experiments carried out on the first of a series of cores built in the zero energy reactor DIMPLE in support of the general investigation of the reactor physics of Steam Generating Heavy Water (S.G.H.W.) reactors which have been undertaken by the Water Reactor Physics Division at A.E.E. Winfrith. The experiments in later cores will be described in further reports. A companion series of papers covering the DIMPLE experiments and the work undertaken in sub-critical assemblies will be issued to compare the experimental data with theoretical predictions based on the methods of calculation in current use at Winfrith.

DIMPLE (Deuterium Moderated Pile, Low Energy) was first constructed at A.E.R.E. Harwell in 1954, and was initially used to study heavy-water moderated lattices including mockups of the DIDO/PLUTO reactors. It was subsequently used with a reactor oscillator to provide basic nuclear data. Its final use at A.E.R.E. was to carry out a preliminary study of S.G.H.W. type reactors (1), (2). The reactor was then dismantled and transferred to A.E.E. Winfrith where it has been rebuilt in a considerably modified and more versatile form.

The first cores which have been studied in DIMPLE at A.E.E. Winfrith are of the S.G.H.W. type. An S.G.H.W. reactor core consists of a calandria (i.e. an unpressurised vessel with numerous "calandria" tubes passing through it), pressure tubes which fit inside the calandria tubes, which themselves contain the fuel in the form of multi-rod bundles of uranium oxide rods canned in some suitable material (see Fig. 5). The power reactor fuel is cooled by light water which leaves the pressure tubes as wet steam. The reactor may contain "superheat" channels to recirculate the steam, separated in the steam drum, through the reactor core.

The experiments described in this report are on a core in which the superheat channels only are simulated in DIMPLE. Air was used in the pressure tubes in lieu of dry steam. The work was undertaken during the period June 17th to August 3rd 1962. Since this report is the first of a series of similar accounts of experimental work, the experimental techniques are described in some detail.

2. Description of DIMPLE as Constructed for this Experiment

2.1 Brief description of the DIMPLE reactor

DIMPLE consists essentially of an aluminium reactor core tank, 8' 6" diameter and 10' high, surrounded by a 2' thick graphite reflector (which may be removed), and enclosed within a biological shield constructed of concrete blocks some 4' thick (Fig. 1). A wide variety of reactor cores may be assembled in the core tank. The liquid moderator (D_2O in this case, but which can be H_2O or an organic liquid) is stored in dump tanks situated in a pit a short way from the reactor tank. Means of pumping the moderator into and dumping the moderator out of the reactor tank are provided. Ancillary plant allows the moderator to be heated quickly from ambient temperatures up to 90°C and cooled again.

The reactor is normally taken to criticality by increasing the bulk moderator level in the core tank, thereby providing a clean core for experiments without control absorber perturbations. Two banks of safety rods are provided (which are stationery either in or out of the core) together with

continuously adjustable coarse and fine control rods if required. Ionisation chambers and BF_3 proportional counters situated in the graphite reflector provide flux instrumentation covering the six decades from 10 to 5.10^7 n/cm^{-2} sec; peak centre core fluxes are about ten times these values.

The safety, control, and interlock circuitry has largely dispensed with electromagnetic relays and consists of a "solid state" dynamic logic system, the first of its type in the U.K. The instrumentation itself is largely "transistorised", and it is intended to make it completely so as soon as practicable. This equipment has been installed to obtain experience on reliability under reactor conditions, and to provide performance statistics before application to larger plant (i.e. power reactors).

A more complete description of the plant is embodied in the DIMPLE Safety Document (3) and an Engineering description (4) which will become available shortly.

2.2 Description of the core

The particular lattice built into DIMPLE for these experiments was similar in many respects (but not in fuel enrichment) to the S.G.H.W. lattice previously studied in DIMPLE at A.E.R.E. Harwell (1). It consisted of 24 fuel channels arranged on a 9.5 inch square lattice pitch, as shown in Figure 2. The pressure and calandria tubes (see Fig. 4) were of aluminium, and their dimensions are given in Appendix I. The fuel (see Fig. 5), which was made up in 14" lengths, consisted of a 90-rod bundle of 0.3" nominal diameter uranium oxide pencils, enriched to 1.79% U235, and canned in 0.036" wall aluminium; it was loaded into the pressure tubes to a total height of 56" (i.e. four lengths).

The safety rods were divided equally into two banks of nine rods, each bank operating in the half of the core adjacent to its pulley shaft. The rods consisted of 1.66" O.D. (20 SWG thick) by 38" long cadmium tubes sandwiched between 20 SWG aluminium tubes. Identical rods were used as fine and coarse control devices. The positions of the rods are shown in Figures 2 and 3.

In order to allow insertion of experimental equipment into the core without breaking into the D_2O circuit, nineteen "search" tubes, of 1.5" nominal internal diameter and 0.015" nominal wall thickness, were positioned interstitially to the fuel (see Figures 2 and 3). These tubes could be flooded with D_2O (to a height corresponding to the main moderator height) from outside the core tank.

Four devices to detect moderator height were situated in the corners of the tank. Two of these, (the Herriott Mk I and II moving probe instruments, based on the conductivity principle) allowed measurement of moderator level differences to ± .1 mm, and absolute measurement to about ± .5 mm. A third device (a float-type Evershed probe) was less accurate but provided signals to the interlocks and safety circuitry. The fourth device, a simple fixed height conductivity probe, was used merely to back up one safety interlock provided by the Evershed probe.

In order to support the lattice structure within the tank various fuel support and lattice plates were fitted. Their position is shown in figure 3 and details are given in Appendix I.

3. Approach to Critical

In most of the cores studied in the SGHW experimental programme the pressure tubes contain moderating "coolant". One of the means of loading such cores is to insert pressure tubes, which have previously been loaded with fuel and "coolant", into the empty calandria. The core could thus be multiplying even when there was no bulk moderator in the main tank. In order to standardise procedures it has been laid down (3) that in all cases multiplication measurements must be made whilst loading fuel, although strictly this is unnecessary in cores with dry fuel. A 10 curie polonium beryllium source and several BF_3 chambers were used for these measurements. There were no substantial changes in the count rates recorded during the fuel loading.

Having loaded the twenty-four pressure tubes with fuel, criticality was approached by raising the level of the D_2O moderator in the reactor tank. The moderator height H was raised in discrete steps and the count rates C from BF_3 chambers situated throughout the core were recorded. H^2/C was plotted against H^2. At suitable points the safety rods were inserted to estimate their effect on multiplication. The reactor was returned to the previous condition, and the normal approach was continued. The effect on multiplication of removing the "in-pile" experimental BF_3 chambers was measured when the reactor was estimated to be about 1% sub-critical, based on the extrapolated critical height and a calculated value of $d\rho/dh$. These were finally removed and the moderator height slowly raised until the reactor was divergent. All the above operations are detailed in reference 3. The moderator level (measured by the MkI Herriott probe) at criticality was 158.45 cm. At this stage, all the search tubes in the core were still empty.

Typical approach curves from "in-pile" and "installed" BF_3 chambers, together with a sketch showing the counter and source positions, are given in Figure 6. It is evident that, as one might expect, those chambers nearest to the source were counting a considerable number of neutrons direct from the source, thus preventing them giving an early prediction of critical height. The outermost chambers, however, give a linear relationship from about half critical height upwards.

To indicate the extent to which the various chambers can be relied on to give early warning of reactivity the value of the effective reproduction constant k_{eff} has been estimated at the "turn-over point" on each graph (see Fig. 6). The values of k_{eff} have been deduced from the critical value of $d\rho/dh$ and the assumption that $d\rho/dh$ is inversely proportional to h^2. This assumption, rather than the more conventional inverse h^3 relationship, was chosen because it is conservative (i.e. over estimates k_{eff}) and it takes some account of the increase of reflector saving (i.e. geometric buckling) with increasing core height, which is most marked in a D_2O moderated core. [The one-group expression for a core of bare height h, core radius R, and radial reflector saving λ is $\frac{d\rho}{dh} = \frac{2M^2}{k_\infty}\left[\frac{\pi^2}{h^3} + \frac{2.405^2}{(R+\lambda)^3}\frac{d\lambda}{dh}\right]$, which varies more slowly than $\frac{1}{h^3}$.]

We conclude, from the values of k_{eff} marked on figure 6, that for large cores of this type in DIMPLE, chambers placed in fixed positions in the core tank, relatively near to the neutron source, are of less value until later on in the approach, and for early predictions we must rely on the results from the "installed" chambers situated in the graphite reflector. All chambers do, however, give adequate notice of the approach of, and position of, criticality, i.e. all graphs reach turn-over point before k_{eff} exceeds 0.96.

4. Reactivity Measurements

4.1 Scale of reactivity

All reactivity measurements have been normalised to a scale based on the steady diverging period of the super-critical reactor. The relationship between period and reactivity used in this work allows for delayed U235, U238, and photo-neutrons in a finite sized reactor (since the delayed neutrons have a lower leakage probability than prompt neutrons). Appendix II gives all the information used to compute this relationship together with a very abbreviated table. The theory will be published separately later, but is in essence that of reference 5.

It would lengthen this report prohibitively to quote the actual doubling times measured in every experiment. It is, however, possible to correct any reactivities quoted to a revised scale of reactivity, should this become necessary, since doubling time measurements were only made in the range 15 to 45 seconds. To a good approximation therefore one may use a factor obtained from the ratio of reactivities on the revised and present reactivity scales corresponding to, say, a 30 second doubling time.

4.2 Measurement of doubling time

The reactor instrumentation is not accurate enough for this purpose. Experimental $\frac{1}{4}$ inch diameter fission chambers were connected to 1430 A head and main amplifiers coupled to 1070 B fast scalers. The output from the fast scaler was connected to two paralleled pairs of 1009 scalers series connected. A switching unit connected to accurate timing pulses automatically starts, stops, and resets each series pair of 1009 scalers in sequence. Thus integrated counts over predetermined time intervals may be observed. When the reactor is diverging with a steady period the logarithm of these counts against time is a linear function from which the doubling time may be computed.

With two such channels in use, the doubling time was measured to ± 1% on most occasions. It was usually possible to obtain a steady period for about two decades of flux rise, after which the dead time of the counting system was apparent in the levelling off of the counts recorded. The period of time between the addition of reactivity ceasing and a steady period being reached depended on the actual period, but was in general the time taken for the flux to increase by about a third of a decade in flux. Fig. 7 gives typical doubling time graphs, the lower diagram demonstrating (at much higher count rates than were used normally) the dead time effect.

4.3 Rate of change of reactivity with moderator height - $d\rho/dh$

The steady period corresponding to several moderator heights above criticality was measured, and the excess reactivity deduced plotted against the height above critical. The slope of the linear plot gives $d\rho/dh$. Fig. 8 illustrates a typical example.

In order to investigate the change of $d\rho/dh$ with moderator height these experiments were repeated at various insertions of the fine control rod. Figure 9 gives the experimental results, which show fairly clearly the effect the end of the fuel has on an otherwise smooth variation. On the same figure we record the critical height versus insertion of the fine control rod. Zero on the fine control rod scale of Figure 9 corresponds to the rod being fully inserted, the bottom of the rod being 38 cm from the tank bottom in this position. Individual measurements of $d\rho/dh$ have a standard deviation of ± 2% estimated from the consistency of the results.

The value of $d\rho/dh$ at the normal critical height (i.e. with fine and coarse rods removed and all search tubes filled with D_2O) was 0.160 ± 0.003% cm^{-1}.

4.4 Fuel element reactivities

Although the majority of the fuel is locked into the reactor by a security cover which is interlocked into the safety circuitry, three previously selected fuel channels are available by opening locked and interlocked access covers.

The pressure tubes containing fuel under these access covers were removed in turn, and the new critical height and $d\rho/dh$ measured. The reactivity controlled was computed from the very simple expression, $\delta h_c \times \frac{d\rho}{dh}$, where δh_c was the change in critical height and $\frac{d\rho}{dh}$ the average of $d\rho/dh$ measured at the two critical heights.

The results of these measurements are given below in Table I. The errors are based on the assumption that each value of $d\rho/dh$ is known to ± 2%. Pressure tube reference positions refer to Fig. 2.

TABLE I

Fuel Element Reactivity

Reactor condition	Critical ht. cm	$d\rho/dh$ % cm^{-1}	Reactivity of fuel channel %
Normal	157.90	0.153	
Pressure tube in J10 removed	163.63	0.125	0.79 ± 0.02
" " " H10 "	162.99	0.131	0.72 ± 0.02
" " " J06 "	163.87	0.130	0.84 ± 0.02
Fuel clusters in J10 "	164.68	0.122	0.93 ± 0.03

We note that the values of $d\rho/dh$ quoted above do not agree (at a given height) with those obtained using the fine control rod to vary reactor height. For example, with J10 missing (critical height 163.6 cm) $d\rho/dh$ was measured as .125% cm^{-1} compared with 0.116% cm^{-1} for the same critical height with the fine control rod inserted to 33 cm (i.e. nearly fully in) and all fuel present. This difference was about 5 standard deviations and was typical of the results obtained (see Fig. 9). Although some difference in $d\rho/dh$ would be expected due to the different method used to change critical height (i.e. a rod partially inserted as opposed to a full length pressure tube removed), it is surprising to find the effect so large, and further theoretical investigation of this effect is clearly necessary.

4.5 Measurements of negative reactivity worths of safety and control rods

The simplest experimental technique is to measure the multiplication of the system directly by means of the count rate registered by a BF_3 counter. Simple theory indicates that the negative reactivity is inversely proportional to the count rate C. In practice as the reactor becomes more sub-critical the flux shape deviates further from the critical flux-shape, and thus the experimental result becomes dependent upon the counter and source position. The interpretation of these measurements is, therefore, not straightforward for values of k_{eff} less than about 0.99.

In order to determine the constant of proportionality between negative reactivity and reciprocal count rate it is necessary to measure the change of count rate when a known reactivity change is made. We have assumed that the reactivity difference between critical heights of the reactor [inferred from doubling-time measurements] corresponding to two settings of the fine control rod is the same as the reactivity difference between these same two insertions of the fine control rod with the moderator level equal to the clean critical height (for which multiplication measurements were made). For an axially unreflected core with a full length control rod, and the two control rod insertions corresponding to fully in and fully out, such an assumption would be rigorous. Although none of the above provisos apply here the change in critical height between the critical and sub-critical experiments was only 4 cm, and any error will hence be small.

Suppose the critical heights corresponding to the two positions of the fine control rod are h_1 and h_2 respectively. Suppose also that with the moderator height equal to the clean critical height these two positions of the fine control rod in turn lead to measured count rates C_1 and C_2 (for any of the experimental counters). Then the constant of proportionality for that counter, $\frac{d\rho}{d(1/C)}$ is given by

$$\frac{d\rho}{d(1/C)} = \frac{\int_{h_1}^{h_2} \frac{d\rho}{dh}\, dh}{\frac{1}{C_1} - \frac{1}{C_2}}$$

Using Figure 9 the integral in the denominator of the right hand side of the above is 0.225% for fine control rod insertions of 60.04 cm and 45.54 cm respectively.

TABLE II

Reactivities Deduced by Sub-critical Multiplication Measurements

Moderator height (cm)	Fine control rod pos'n (cm)	Safety rod positions	Negative reactivities % deduced from counters (see Fig.7) arranged in order of distance from source						
			ChII	ChIII	ChIV	ChI	Log A	Log B	Linear
158.6	60.04	OUT	0.752	0.712 0.744	0.723 0.753	0.719 0.760	0.763 0.783	(0.648) (0.693)	0.73 0.74
"	45.53	"	0.527	0.503	0.513	0.515	0.548	(0.446)	0.51
158.7	99.8	Bank A IN	8.7	6.4	5.9	7.1	9.0	(5.6)	4.4
"	"	Both Banks IN	22.6	20.0	15.7	19.5	12.7	(9.4)	10.2
"	"	Bank B IN	-	10.7	9.5	9.3	5.2	(4.5)	7.1
121.9	OUT	OUT	8.9	8.3	7.7	7.2	5.2	(4.4)	5.7

It is difficult to draw more than qualitative conclusions from these results. The results from Log channel B, although quoted, were suspect since the equipment was giving trouble at the time.

We notice that

(a) <u>The reactivity predicted was lower the further the detector was from the source</u>.

(b) <u>The chamber in the reflector adjacent to an inserted bank of rods registered a larger change of count rate, and hence a larger reactivity, than one placed diametrically opposite</u>.

Observation (b) may be understood fairly simply, since the introduction of a markedly asymmetric sink of neutrons will depress the flux in its vicinity. Unfortunately, however, it is the change of multiplication of the fundamental (and symmetric) component of the flux distribution which determines the reactivity change we wish to know. Under these conditions the higher harmonic components will have been so predominant that it is doubtful whether any chamber registered the required results.

Observation (a) was contrary to expectation if the variation with detector position were due to a component of the recorded flux coming directly from the source. In an ideal case a detector placed such that the reactor presented a point source to it (i.e. at infinity) should register true changes in reactivity. The chambers sited in the reflector were far from this ideal.

To sum up, therefore, the method of sub-critical multiplication is not ideal for the evaluation of control or safety rod worths, but it was considered reasonable to use the lowest recorded value to satisfy the DIMPLE safety criteria (3) (i.e. the reactivity worth of the least reactive bank of safety rods, allowing for loss of 20% of the rods, must be greater than 1.6%).

A better technique for this measurement would be to measure the prompt neutron decay constant after applying a pulse of neutrons to the sub-critical reactor. This technique measures the harmonic with the highest k_{eff} (i.e. the fundamental) and should be independent of source and detector positioning. Work on this technique is planned for the future.

4.6 Miscellaneous reactivities

Up to this point in time all 19 search tubes had been empty. The change of critical height on filling firstly the centre twelve (in the core proper) and then all but the two outermost was measured. The tubes then remained filled.

Following this the reactivities controlled by (a) a 12EB40 BF_3 counter and (b) a $\frac{1}{4}$" diameter fission chamber covered by a .040" thick by 17 cm long cadmium sleeve were measured when these were inserted in turn into a search tube near the core centre. The final measurement was of the effect of the coarse control rod.

TABLE III

	Reactor condition	Critical height (cm)	Measured $d\rho/dh_{=1}$ % cm	Reactivity change from normal %	Remarks
a	Normal	158.03	.154	-	
b	Centremost 12 search tubes filled with D_2O	155.69	-	+ 0.367	
c	All search tubes except K03 and C15 filled with D_2O	155.46	.160	+ 0.403	Reactor in this state for remainder of experiments
d	(c) plus cadmium sheathed fission chamber in centre	156.00	-	- 0.086	
e	(c) plus BF_3 counter in centre	155.90	-	- 0.070	
f	(c) plus coarse control rod fully in	156.30	-	- 0.134	

We conclude, therefore, that the clean critical height was 155.46 cm (strictly slightly under this due to the effect of the two measuring fission chambers in K03 and C15, although their effect was much less than 0.05 cm).

5. Macroscopic Reaction Rate Distributions

5.1 Introduction

This section describes measurements made using $\frac{1}{4}$" diameter rigid stemmed fission chambers inserted into flooded (i.e. D_2O filled) search tubes. Three types of fission chambers were used, 10' long and 5' long U235 coated, and 5' long Pu239 coated. The epi-cadmium reaction rates were determined by surrounding the active regions of the chambers by 0.040" thick by 17 cm long cadmium sleeves. Fig. 11 illustrates the arrangement. Note that the cadmium sleeve overlaps the active region by 12 cm.

The reactor flux was monitored using a similar chamber set up to switch the experimental counters off after a pre-determined count. As a general rule at least three separate counts were made at each position, the total number of counts recorded being well in excess of 10^5 at each position. A subsequent statistical check on one channel indicated that the drift of the electronics contributed a random error ~0.1% in this case, and thus the ratio of experimental counts to monitor counts on an individual reading would have a 0.14% random error even with infinite count rates. From measurements carried out more recently it was estimated that the dead time of the counting equipment was about 1.5 ± .5 sec. The counting rates employed meant that in some cases the dead time correction was appreciable (up to 5%) and had to be taken into account in the analysis of the results.

From the measurements made a number of reactor parameters were deduced as follows:-

(a) From measurements using one chamber in one search tube at different heights, both bare and cadmium covered, results from the axial region with constant cadmium ratio were used to determine the axial component of buckling.

(b) From measurements using several chambers sited in turn in all the search tubes at a constant axial position the radial bare and cadmium covered reaction rates were measured. The radial component of buckling was deduced from the results within the region of constant cadmium ratio.

(c) By measurements using chambers with different fissile materials in the same position in the core, both bare and cadmium covered, the cadmium ratios were deduced absolutely, and the uranium to plutonium reaction rates relative to a standard spectrum. The spectrum generated in the NESTOR graphite thermal column was used as the standard (6), since the 5' long chambers had been previously calibrated in this spectrum (7).

Appendix III summarises the radial measurements, and some distributions are plotted in Figure 12. Appendix IV summarises the axial measurements and the axial distribution is plotted in Figure 13.

5.2 Spectrum results

Examination of the results in Appendix III shows quite clearly that the region of constant spectrum in this core is extremely small. The search tubes situated two lattice pitches (48.26 cm) from the core centre are in a softer spectrum than the equilibrium one, but the search tubes at half this radius are, within experimental errors, in the same spectrum as that at the core centre. We have therefore assumed that the measured (i.e. uncorrected) equilibrium spectrum of the reactor is characterised by the mean of the results in search tubes K11 and K13 (Figure 2) and is as follows:-

$$\text{U235 Cadmium Ratio} = 21.23 \pm 0.60$$

$$\text{Pu239 Cadmium Ratio} = 30.74 \pm 0.65$$

$$\frac{\text{Pu239/U235 ratio in reactor}}{\text{Pu239/U235 ratio in NESTOR thermal column}} = 1.218 \pm 0.008$$

To arrive at the errors (standard deviations) quoted above we have assumed initially that they are due to two sources:-

(a) Normal counting statistics.

(b) An amplifier gain drift error of 0.1% for each individual measurement.

Based on the analysis (Appendix III) of many measurements taken in a single search tube, the error computed above was increased, by a factor of $\sqrt{2}$, which allows for the extra error possibly attributable to positioning in the search tube. Finally (particularly important for the cadmium ratio results) allowance for a 33% uncertainty in the assumed dead time of 1.5 μ sec was made.

The Pu239/U235 ratio in the NESTOR thermal column is quoted to be 0.357 ± 0.001 (7) and has been remeasured recently (May 1963) to be 0.3514 ± .0009. We have used the latter figure as it is the one measured nearest to the time of the experiments. The difference between the two values could be due to gas leakage in the chambers.

The method of setting the counters up to ensure a given efficiency at all times is described in detail elsewhere (7) and consists of a technique which sets the descriminator bias accurately at some chosen point of the neutron energy spectrum independent of gain changes in the counting equipment used. The results reported above have had no corrections made for attenuation of flux by the fission chamber walls and active coating, or the effect of displacing the D_2O by the fission chamber. The method of making the former corrections is also described in ref. (7).

5.3 Radial component of buckling β^2

Since the spectrum is constant for search tubes K09, K11, and K13 only, the radial buckling has to be deduced from these points alone. The error in this buckling is hence very dependent upon the accuracy with which the ratios of reaction rates of K09/K11 and K13/K11 may be measured.

In Appendix III, Table III and the text that follows an analysis of all the measurements in these three positions has been made. There is a barely significant difference between the results from K09 and those from K13. The analysis shows that errors other than those due to counting statistics and counter drift are present which in themselves are comparable to the known errors. Taking this into account, allowing for a systematic error in the dead time correction applied, and taking a mean of all results from K09 and K13, we obtain a flux ratio between these and K11 of 0.9530 ± 0.0012.

This ratio may be used to deduce the buckling component in the radial direction only if we assume that the macroscopic variation of flux is truly a Jo Bessel function. The core is small and not by any means cylindrical (see Fig. 1). Assuming that it is a Jo, however, and allowing for a 1% standard deviation in the radial position (consistent with the small and barely significant difference in the measurements in K09 and K13) we obtain:-

$$\beta^2 = 3.26 \pm 0.11 \ m^{-2}$$

In order to illustrate how dependent we are on the assumption that the core approximates to a cylinder it is instructive to work out β^2 on the assumption that the core was of square section, and the flux cosinusoidal. On this assumption $\beta^2 = 3.24 \ m^{-2}$.

The random error (standard deviation) quoted on β^2 is thought to be realistic because

(a) It takes account of the observed asymmetry in the core between K13 and K09.

(b) Measurements outside the region of constant cadmium ratio show that the asymmetry is less rather than greater at these points (see Appendix III, Table I).

(c) Measurements in later cores (which will be published later) containing a larger region of constant spectrum have demonstrated that the values of β deduced from measurement at small radius were consistent with those at larger radius.

(d) The value of β is independent of the functional form (Jo or cosine) used to fit the observed reaction rates.

What cannot, however, be accounted for in the above quoted error is the uncertainty as to whether a measurement in such a small core may be applied with validity to a larger (perhaps less well reflected) core.

As there has been some evidence that bowing of search tubes can lead to large errors in the reaction rate ratios in S.G.H.W. lattices in other plant at Winfrith, an experimental check was made by rotating the search tubes in K09, K11, and K13. The change of count rate was within the expected errors of counter drift and normal statistics, and it was therefore deduced that this effect was not the cause of this discrepancy. Although the discrepancy between K09 and K13 has been attributed to an error in radial positioning in

computing β^2, such an error (in the absence of bowing) was outside the engineering tolerances to which the lattice plates have been made. More recent work (which will be reported in a later report of this series) has demonstrated that an apparent positioning error may be reversed by exchanging pressure tubes complete with fuel, and it is therefore more likely that the observed discrepancy was due to a combination of cluster to cluster variations of fuel and bowing of pressure tubes.

5.4 Axial component of buckling α^2

The axial variation of flux was measured in search tube K11, both with a bare and with a cadmium covered U235 fission chamber. The chamber was connected to a calibrated rod which protruded through a gap in the top reactor shield. This enabled an operator to move the chamber (which controlled very little reactivity) without reducing reactor flux. (The deficiency in the shielding was made good by special portable shielding blocks designed to hang on the edges of the permanent shields.)

The results of the scans have been fitted to an expression of the form $\phi_i = A \cos \frac{\pi}{H} (z_i - z_o)$.

Where $(\pi/H)^2$ is the axial component of buckling

z_i is the position of the detector in the i^{th} measurement

z_o is the centre of symmetry of the flux distribution

ϕ_i is the measured reaction rate of the fission chamber

Values of A, H, and z_o were deduced by minimising the magnitude of the function χ^2 where

$$\chi^2 = \sum_i \frac{[\phi_i - A \cos \frac{\pi}{H} (z_i - z_o)]^2}{\text{Var } \phi_i}$$

A computor programme was used which accepts as input the experimental counts, monitor counts, time of counting, counter dead time, estimates of chamber positional errors both axially and radially, and the error due to counter drift. It computes the variance on each point (Var ϕ_i) due to these factors and uses the inverse variance to weight each point.

The initial fits were made using all points within the core boundary. Examination showed that there were systematic misfits close to the cluster ends and the final estimates were obtained using only those points indicated in Tables IV 1 and IV 2 of Appendix IV. The procedure to arrive at this final fit was successively to reject measurements at systematically increasing distances from the cluster ends until the value of χ^2 approached the expected value (i.e. the number of degrees of freedom) or the value of χ^2 on individual points fell below 9 (i.e. the discrepancy was less than three standard deviations). For consistency both bare and cadmium covered results were rejected simultaneously, although Table IV 1 (cadmium covered) shows that certain of the points could have been re-introduced into the fit. Final values of H, z_o, and χ^2 (expected value equal to the number of degrees of freedom or n-3, where n is the number of points used in the fit) were as follows:-

	Dead time assumed	H	z_o	χ^2	Degrees of freedom	Probability of this χ^2 being exceeded in normal sampling
Bare	Zero	168.3 ± .3	107.9 ± .1	28.5	6	<1%
Cd covered	"	168.2 ± .3	107.3 ± .1	13.0	6	5%
Bare	1.5×10^{-6} sec	165.1 ± .2	107.7 ± .1	16.1	6	1%
Cd covered	"	166.7 ± .2	107.3 ± .1	8.3	6	30%

The experimental results are recorded in Appendix IV and plotted in Figure 13. As was expected the aluminium cluster ends influence the axial distribution to a considerable extent. The effect of the 3.6 cm gap in the uranium oxide between fuel clusters was to increase the U235 total reaction rate in the vicinity, and to decrease the cadmium covered U235 reaction rate. Figure 13 shows this effect quite clearly.

The "goodness of fit" for the bare results is worse than would be expected from the statistics, but is satisfactory for the cadmium covered results. If we examine Figure 13 it is obvious that this is due to the perturbations of the end fittings extending throughout the whole height of the reactor. The result from the cadmium covered scan will therefore give a more reliable estimate of the buckling.

Before deducing the axial buckling, however, we need to correct the fitted "height" for the reactivity of the cadmium covered chamber. With this chamber at the bottom of the search tube the critical height was 0.4 cm higher than when it was at the top (i.e. removed) and when at the centre it was 0.7 cm higher. [The total change for the bare scan was only 0.15 cm and may be neglected.] The cadmium covered results are, therefore, obtained under changing critical height conditions, but it would appear reasonable to correct the observed height by one half the maximum change in critical height observed (i.e. 0.4 cm). Thus H_{cd} becomes 166.3 ± .2 cm. Since the bare result is a poor fit to a cosine we must reduce its weight compared to the cadmium covered result. Figure 13 shows that the deviation of ϕ_{obs}/ϕ_{calc} from unity is 3% for the bare scan but only 0.5% for the cadmium covered scan. Assuming the under cadmium width to have six times the weight of the bare width, the mean width was 166.1 ± .2 cm. The error was then increased by 0.45 cm to allow for an estimated 33% error in the assumed dead time of 1.5 μsec.

Hence $H = 166.1 \pm .5$ cm

$\alpha = 1.891 \pm 0.006\ m^{-1}$

$\alpha^2 = 3.576 \pm 0.023\ m^{-2}$

From Appendix IV the mean bottom and top reflector savings may be estimated as 23.7 cm and 3.6 cm (allowing 0.4 cm off for the cadmium covered result) respectively. The sum of the two reflector savings has an error equal to that on H (i.e. ± .5 cm).

The error on a^2 quoted above is based on the internal consistency of measurements made in the centre of the reactor only. In later cores (see later reports of this series) axial measurements were made in more than one radial position and analysis of these has shown no variation of a^2 with radius outside the errors based on internal consistency. We have therefore no reason to believe that the error quoted is, for this reason, too low. However, before comparing these results with theory, one must carefully consider whether the flux distributions in a lattice which has large periodic axial perturbations can be used to deduce a buckling. In the absence of such consideration it is recommended that the error quoted should be increased appropriately. (See conclusions, section 8.)

6. Fine Structure in the Thermal Neutron Distribution

Measurements were made in the lattice cell surrounding fuel element J10. The centre of the fuel element was situated at 17.06 cm radius from the core centre.

One-quarter inch diameter by 0.005 inch thick manganese nickel alloy foils (containing 12% Mn by weight) were used, situated in the tie rod, between fuel pellets inside demountable fuel cans, on the outside surface of the pressure tube, and on the inside surface of the calandria tube. Similar foils were attached to the DIMPLE foil machine (2). The foils were arranged in two planes 11.6 cm apart, the height of the planes being such that the foils were in a region remote from the end of the fuel element clusters. Figure 14 shows the arrangement of the foils in the reactor. The final mean experimental results are shown in Figure 15.

Two irradiations were carried out, and hence, with two layers of foils per irradiation, four separate estimates of the fine structure were obtained. Appendix V summarises the results from these experiments, and corrects the results for foil calibration factors, macroscopic variation and axial variation. The last named correction was necessary because of an error in the relative axial positioning of the foils in the moderator to those in the fuel. Since at the time of the measurement it had been thought that fuel and moderator foils were in the same horizontal plane, and the error was only discovered some time later, a small doubt exists as to whether the correction applied is right, and hence the normalisation between fuel and moderator results should be treated with reserve.

The results within the fuel are quite satisfactory but those in the pressure and calandria tubes show a greater variation from run to run. Since the calandria foil was attached to the pressure tube by means of a phosphor-bronze spring (see Figure 14), and the pressure tube was lowered into the calandria tube, the radial positional accuracy was much less than all other foils. The foils in the moderator were positioned on the foil machine described in reference (2) and their positional accuracy was also somewhat suspect. The foils in the fuel (0.25" diameter sandwiched between 0.3" pellets) were carefully positioned by eye concentric to the pellets.

The errors quoted are based upon the consistency from set to set, since the counting errors are obviously only a very small proportion of the total observed spread. Each foil was counted for something like 10^6 counts. The foils were unfortunately not calibrated until after the reactor irradiations and due to pressure of other work only two calibrations were completed.

9. Acknowledgements

The Authors wish to acknowledge the great efforts and long hours put in by members of Low Power Operations Group, General Engineering and Operations Division, and the team from Design and Manufacturing Division, when building and commissioning the plant to a very tight time-scale. We also wish to thank Mr. G. W. Watson and the DIMPLE operations team, the DIMPLE Maintenance team, and Messrs. Whyard, Page, and Keats, of Control and Instrumentation Division, who worked very hard to keep the reactor running during considerable teething troubles in the early weeks of operation. Finally thanks are due to the members of Experimental Physics Group, Water Reactor Physics Division, mentioned on the title page, who assisted with the experiments and their analysis.

References

1. AERE-M 727. First Report on the S.G.H.W. Experiment in DIMPLE. Edited by J. W. Hilborn.

2. AEEW-R 82. Second Report on the S.G.H.W. Experiment in DIMPLE. H. R. McK.Hyder, et al.

3. AEEW-M 329. The Safe Operation of DIMPLE at A.E.E. Winfrith. Part I - Description and Operation with S.G.H.W. type cores containing only uranium fuel. G. M. Wells.

4. DIMPLE Engineering Handbook. (In course of preparation.)

5. AERE R/R 2464. The establishment of a doubling time scale of reactivity for thermal reactors. J. Codd and G. M. Wells.

6. NUC/P11. Neutron spectrum and flux measurements in the NESTOR Thermal column compared with a 6 foot cube of graphite. J. P. Hardiman and E. J. Maunders.

7. AEEW-M 295. Reactor Physics of Hydrogen moderated systems in HELEN I and II by A. J. Briggs, C. T. Chudley, I. Johnstone, W. H. Taylor.

8. AEEW-M 313 by W. N. Fox, et al. (In course of publication.)

9. AEEW-R 79. Exponential experiments on graphite lattices fuelled with clusters of UO_2 rods. P. E. Francois, R. Hobday, P. J. Lloyd, and D. B. McCulloch.

Appendix I

Details of Core Materials

1. Nominal volumes of materials in regions other than the core (see Fig. 3)

These volumes have been computed from the Engineering drawings and must inevitably be somewhat imprecise due to welds, etc. They are, however, useful as guidance to calculations on overall reactor properties.

Region (See Fig. 3)	Material	Description	Volume (cc)	Percentage volume of region
F	Graphite	Reflector blocks	39×10^5	89.4
	Steel	Webs and base plate for reactor tank	2.5×10^5	5.6
	Aluminium	Fins and reactor tank bottom	2.2×10^5	5.0
C	Aluminium	Fuel support plate Centralising pin, bush, and plate Level probes	93743 1762 125	16.1
		Total Aluminium	94630	
	D_2O	In reactor tank	4.95×10^5	83.9
B	Aluminium	Section of lower lattice plate 13 lengths of search tube 11 lengths of safety rod guide tube 3 lengths of level probe	59400 412 834 79	10.7
		Total Aluminium	60725	
	D_2O	In reactor tank	5.09×10^5	89.3
A	Aluminium	Part of ribs of lower lattice plate 9 lengths of search tube 9 lengths of safety rod guide tube Centralising pin 24 lengths of calandria tube 24 lengths of pressure tube 24 canister base supports for fuel	4541 259 359 120 4866 3334 3938	14.8
		Total Aluminium	17417	
	Air	Inside 24 pressure tubes Between the 24 pressure and calandria tubes	18164 5093	19.7
		Total Air	23257	
	D_2O	In reactor tank	7.71×10^4	65.5
D	Aluminium (over and above that in region E – the normal core)	Lower lattice plate and upper ribs Centralising pin	8885 90	10.2
		Total excess Aluminium	8975	

2. Nominal areas of materials in regions above the bottom reflector

Region G (D_2O side reflector)

Total cross-sectional area	= 3.87×10^4 cm^2
Cross-sectional area of 13 search tubes	= 6.1 cm^2
Average cross-sectional area of 11 safety rod guide tubes	= 13.8 cm^{2*}

Region E (normal core)

Total cross-sectional area	= 1.40×10^4 cm^2
Cross-sectional area of 9 search tubes	= 4.2 cm^2
Average cross-sectional area of 9 safety rod guide tubes	= 11.3 cm^{2*}
Inner radius of pressure tube (Aluminium)	= 6.660 cm
Outer radius of pressure tube (")	= 6.985 cm
Inner radius of calandria tube (")	= 7.926 cm
Outer radius of calandria tube (")	= 8.414 cm

Fuel - see section 4 of this Appendix.

3. Measured weights, densities based upon nominal dimensions, and neutron absorption cross-sections relative to Aluminium standard of GLEEP (230 mb at 2200 m/s)

Item	Measured weight (gm)	Nominal volume (cc)	Nominal density	Neutron cross-section relative to GLEEP standard (0.00508 cm^2/gm)	
Fuel support plate	$(2.24 \pm .2) \times 10^5$	9.37×10^4	$2.4 \pm .2$		
Lower lattice plate	$(1.93 \pm .2) \times 10^5$	7.28×10^4	$2.7 \pm .3$		
Complete search tube 379 cms long	590 ± 10				
40 cms of centre of search tube	52 ± 2	18.6	$2.8 \pm .1$		
* Complete safety rod guide tube (327 cm long)	(4 off) 1709 ± 2				
	(16 off) 1144 ± 5				
(Deduced from above)	4.53 ± 0.1	1.78	$2.6 \pm .1$		
1 cm of slotted barrel of safety rod guide tube	2.73 ± 0.1	1.12	$2.4 \pm .1$		
Complete pressure tube	(20 off) $(1.45 \pm .01) \times 10^4$			1.053	$\pm \frac{1}{2}\%$
	(4 off) $(1.45 \pm .01) \times 10^4$			1.031	
1 cm of centre part of pressure tube	$37.5 \pm .3$	13.93	$2.7 \pm .1$	1.053	
Complete calandria tube	(20 off) $(2.52 \pm .02) \times 10^4$			1.053	
	(4 off) $(2.52 \pm .02) \times 10^4$			1.028	
1 cm of centre part of calandria tube	$66.6 \pm .6$	25.05	$2.7 \pm .1$	1.053	

*The existence of two thicknesses of tube has only recently been discovered, and the positions of individual tubes was not recorded. One may only therefore use a weighted mean in all positions.

Note: The weights of fuel support and lower lattice plates quoted were obtained using two spring balances attached to cables slung to the plates. Thus the readings of the spring balances needed to be corrected by the cosine of their angle to the vertical. The results are hence believed to be accurate to within about 10%.

The errors on the other items are based on the spread of sample results.

4. Details of the fuel cluster (see Fig. 5)

Each channel comprises four cluster frames sitting one upon the other. The details of each cluster frame are as follows:-

Cluster frame component	Mass* (gm)	Nominal Diameter (cm)	Nominal Height (cm)	2200 m/s x-section cm^2/gm
Aluminium top plate	418.1	13.19	2.38	
Aluminium bottom plates	289.4	13.19	1.51	
Stainless steel tie rod plus nut	330.5	1.243	33.5 (rod only)	0.0327
Six stainless steel screws	6.5	-	-	-

Total nominal assembled height of cluster frame 35.56 cm (compared with average measured height of one channel of 35.68 cm).

*From page 11 of reference (1).

Each cluster frame contains ninety fuel pencils, each fuel pencil being as follows (largely from reference 9).

	Nominal	Measured
(1) Pencil length	35.05 ± .10 cm	
(2) Fuel length	32.00 ± .13 cm	
(3) Total weight of pencil	-	177.6 gm (mean of 5250)
(4) No. of pellets per pencil	42	
(5) Mean pellet length	0.762 ± .003 cm	
(6) Mean pellet diameter	0.759 ± .003 cm	0.760 ± .002 cm
(7) Weight of oxide per pencil	153.2 ± .2 gm	
(8) Mean oxygen/uranium Atomic ratio	2.14	
(9) Isotopic abundance as % U235 w/w	1.800 ± .0054	
(10) Thickness of Aluminium can	0.091 ± .008 cm	
(11) Outside diameter of Al can	0.960 ± .023 cm	0.958 ± .005 cm
(12) Mass of can	-	24.4 gm (From (3) and (7))
(13) Neutron absorption cross-section of can relative to GLEEP Al standard		1.021

Note: Reference 9, Appendix II, lists the uranium impurities, but these are not repeated here.

The pencils are arranged in the cluster with their centres on circles of the following radii:

Radius (cm)	No. of pencils
0	1 (tie rod)
1.321	6
2.489	12
3.658	18
4.851	24
6.020	30

5. Properties of D_2O

Nominal isotopic purity 99.7%.

Samples tested had measured isotopic purities ranging from 99.725% to 99.715% during the experiment. The accuracy of the measurement is thought to be to ± 0.003%.

Appendix II

Period-Reactivity Relationship

Following similar arguments to those of reference (7) one may show that, for a system containing U235, U238, and photo-delayed neutrons, the relationship between reactivity ρ and doubling time T is of the form:-

$$\rho = \frac{1}{\left(1 + \frac{\tau_p}{T}\right)} \left\{ \frac{\tau_p}{T} + x_n \left(F_5 \beta_5 \sum_i \frac{a_{i5}/a_5}{1 + T/\tau_i} + F_8 \beta_8 \sum_j \frac{a_{j8}}{a_8} \Big/ 1 + \frac{T}{\tau_j} \right) + x_\gamma F_\gamma \beta_\gamma \sum_m \frac{a_{m\gamma}/a_\gamma}{1 + T/\tau_m} \right\}$$

where τ_p is the prompt neutron half-life.

τ_i, τ_j, τ_m are the delayed neutron half-lives of the i^{th}, j^{th}, and m^{th} precursors in U235, U238, and fission products respectively.

F_5, F_8, are the fractions of fission neutrons born in U235 and U238 which enter the "slowing down" region.

F_γ is the fraction of fission product γ's which produce photo-neutrons in the reactor relative to the fraction which would produce photo-neutrons when emitted from a point source of fission products in an infinite sea of D_2O.

β_5 and β_8 are the delayed neutron fractions in U235 and U238.

β_γ is the number of photo-neutrons produced, per fission neutron emitted from a point fission source in an infinite sea of D_2O, which enter the "slowing-down" region.

x_n and x_γ are the non-leakage probabilities in the reactor, for delayed fission neutrons and photo-neutrons respectively, relative to the non-leakage probability for prompt fission neutrons.

a_{i5}/a_5, etc, are the fractional delayed neutron abundances from the i^{th} precursor in U235, etc.

Note also that the effective delayed neutron fraction,

$$\beta_{eff} = x_n (\beta_5 F_5 + \beta_8 F_8) + x_\gamma \beta_\gamma F_\gamma$$

The data used were as follows:-

U235 β_5 = 0.006444		U238 β_8 = 0.0157		Photo-neutrons β_γ = 0.0012025	
τ_i	a_{i5}/a_5	τ_j	a_{j8}/a_8	τ_m	$a_{m\gamma}/a$
55.72	0.033	52.38	0.013	1105000	0.0004
22.72	0.219	21.58	0.137	190800	0.0008
6.22	0.196	5.00	0.162	15840	0.0033
2.30	0.395	1.93	0.388	5940	0.0233
0.61	0.115	0.49	0.225	1620	0.0208
0.23	0.042	0.172	0.075	462	0.0333
				144	0.0699
				41	0.1996
				2.5	0.6486

F_5 = 0.9683
F_8 = 0.0317
F_γ = 0.25 [Value used in DIMPLE at A.E.R.E. - very arbitrary therefore and may well be larger in this sort of system.]
x_n = 1.049
x_γ = 1.022
τ_p = 1.4×10^{-4} sec. (i.e. lifetime $\sim 2 \times 10^{-4}$ sec.)
β_{eff} = 0.007098

Table of Values

Doubling time (sec)	ρ%	Doubling time (sec)	ρ%
5	0.3204	40	0.1063
10	0.2363	50	0.0912
15	0.1923	60	0.0800
20	0.1639	70	0.0714
25	0.1437	80	0.0645
30	0.1283	90	0.0590
35	0.1162	100	0.0543

Appendix III

Radial Scan Results

Five different $\frac{1}{4}$" diameter rigid stem fission chambers were used for these measurements. Results are expressed, for macroscopic scans, relative to the centre search tube K11, each counter being positioned at least once in this tube during a scan. The 10' long chambers were positioned with their active region ~317 cm from the top of the search tube gland, corresponding to a height from the tank bottom of ~74 cm, which is roughly midway up the second fuel cluster (see Fig. 3). The 5' long chambers were similarly placed but with less precision axially (~ ± .5 cm). Since however the position chosen was very nearly in the centre of the axial flux distribution no appreciable axial positioning error should be evident, and this has in fact been neglected.

Table I summarises the measurements of relative macroscopic U235 and Pu239 reaction rates. Table II summarises the "spectrum" results, which were obtained in similar fashion. Table III provides results in more detail for the centre three search tubes. In all cases the ratios have been corrected assuming a 1.5 microsecond paralysis time, although uncorrected ratios are shown in brackets. The standard deviation on a measurement assumes

(a) Variance on count N = N.

(b) The counter drift introduces a 0.1% standard deviation per count, regardless of the time or number of counts. The expression used to compute the variance (i.e. the square of the standard deviation) is

$$\bar{\phi} = \frac{\bar{C}_1}{\bar{C}_o} \frac{\bar{M}_o}{\bar{M}_1}$$

$$\text{Var } \bar{\phi} = \bar{\phi}^2 \left\{ \frac{1}{n_1 \bar{C}_1} + \frac{1}{n_o \bar{C}_o} + \frac{1}{n_1 \bar{M}_1} + \frac{1}{n_o \bar{M}_o} + 2 \times 10^{-6} \left(\frac{1}{n_o} + \frac{1}{n_1} \right) \right\}$$

where $\bar{C}_1$ and $\bar{M}_1$ are the mean counts from the measuring chamber and the monitor chamber respectively, there being n_1 measurements involved in each mean,

and $\bar{C}_o$, $\bar{M}_o$, and n_o are the same factors when the measuring chamber is in the standard position (i.e. K11).

Table I

Summary of Radial Macroscopic Reaction Rate Measurements (figures in brackets are results uncorrected for dead time)

Position	Radius (cm)	U235 Measurements Bare						Pu239 Measurements Bare				U235 Measurements under Cadmium								Pu239 Measurements under Cadmium					
		Ratio	% S.D.	Ratio	% S.D.	Ratio	% S.D.	Ratio	% S.D.	Ratio	% S.D.	Ratio	% S.D.	Ratio	% S.D.	Ratio	% S.D.	Ratio	% S.D.	Ratio	% S.D.	Ratio	% S.D.	Ratio	% S.D.
K09	24.13	0.9466 (0.9476)	0.53									0.9585 (0.9588)	0.21												
K13		0.9439 (0.9448)	0.53	0.9550 (0.9558)	0.23	0.9543 (0.9575)	0.11	0.9580 (0.9583)	0.25	0.9551 (0.9566)	0.13	0.9300 (0.9306)	0.20	0.9535 (0.9536)	0.36	0.9555 (0.9557)	0.25	0.9543 (0.9553)	0.11	0.9382 (0.9382)	0.63	0.9502 (0.9502)	0.22	0.9434 (0.9434)	0.41
K07	48.26	0.8234 (0.8262)	0.53	0.8297 (0.8294)	0.24			0.8102 (0.8115)	0.27			0.7978 (0.7991)	0.20												
K15	"	0.8238 (0.8265)	0.53	0.8267 (0.8324)	0.24			0.8084 (0.8098)	0.27			0.7776 (0.7780)	0.20							0.7777 (0.7777)	0.66				
O11	"	0.8234 (0.8261)	0.53									0.7777 (0.7781)	0.20												
C11	"	0.8280 (0.8307)	0.53									0.7906 (0.7919)	0.20												
C13	54.05	0.9479 (0.9488)	0.53									0.6284 (0.6303)	0.20												
C15	68.29	1.1414 (1.1385)	0.53									0.2740 (0.2756)	0.23												
K05	72.39	0.9158 (0.9173)	0.53									0.3962 (0.3982)	0.22												
K17	"	0.9100 (0.9115)	0.53	0.9250 (0.9263)	0.25			0.8424 (0.8435)	0.26			0.3919 (0.3939)	0.24	0.3971 (0.3973)	0.48										
E11	"	0.9106 (0.9121)	0.53									0.3865 (0.3884)	0.22												
E13	76.25	1.0106 (1.0104)	0.53									0.2399 (0.2413)	0.40												
C17	86.87	0.9411 (0.9421)	0.53									0.0305 (0.0306)	4.3												
K19	96.52	0.7907 (0.7916)	0.53	0.8247 (0.8275)	0.24			0.6834 (0.6853)	0.30			0.0346 (0.0349)	4.1												
C11	"	0.7721 (0.7755)	0.53									0.0352 (0.0355)	4.1												
C13	99.40	0.7080 (0.7119)										0.0200 (0.0201)	5.2												

Table II

Summary of Radial Plutonium and Uranium Reaction Rate Ratio Results
(figures in brackets are uncorrected for dead time)

Pu/U is the ratio of plutonium to uranium counts with fission chambers bare.
R_5 is the ratio of bare to cadmium covered counts with the U235 chamber.
R_9 is the ratio of bare to cadmium covered counts with the Pu239 chamber.

Position	Pu/U in DIMPLE		R_5		R_9	
	Result	% S.D.	Result	% S.D.	Result	% S.D.
K11	0.4220 (0.4411)	0.15	21.23 (19.66)	0.21	30.74 (29.67)	0.28
	0.4390 (0.4438)	0.25				
K13	0.4223 (0.4407)	0.15	21.20 (19.70)	0.22	31.18 (30.09)	0.30
	0.4405 (0.4450)	0.25				
K15	0.4278 (0.4318)	0.25				
K07	0.4303 (0.4343)	0.25				
K17	0.3999 (0.4042)	0.26				
K19	0.3638 (0.3675)	0.27				
NESTOR Thermal Column	0.3514	0.25				

Table III

Summary of Measurements in K09 and K13

Position	Fission chamber used	Bare or cadmium covered	Uncorrected ratio ø	Corrected ratio ø	% standard deviation
K09	10' U235	Bare	0.9534	0.9506	0.12*
	"	"	0.9566	0.9538	0.12*
	"	"	0.9548	0.9520	0.11*
	"	"	0.9524	0.9494	0.11*
	"	"	0.9536	0.9507	0.11*
	"	"	0.9476	0.9466	0.53
	"	U/C	0.9588	0.9585	0.21
K13	10' U235	Bare	0.9567	0.9539	0.12*
	"	"	0.9580	0.9555	0.12*
	"	"	0.9448	0.9439	0.53
	5' U235	"	0.9558	0.9550	0.23
	"	"	0.9575	0.9543	0.11
	5' Pu239	"	0.9583	0.9580	0.25
	"	"	0.9566	0.9551	0.13
	10' U235	U/C	0.9306	0.9300	0.20
	5' U235	"	0.9536	0.9535	0.36
	"	"	0.9557	0.9555	0.25
	"	"	0.9553	0.9543	0.11
	5' Pu239	"	0.9382	0.9382	0.63
	"	"	0.9502	0.9500	0.22
	"	"	0.9434	0.9434	0.41

*Not recorded in previous table

Weighting each point with its inverse variance we have, for the corrected ratios,

K09 Mean = 0.9516, χ^2 = 20.5, Degrees of freedom = 6
Weighted S.D. =

K13 (except point) Mean = 0.9541, χ^2 = 23.3, Degrees of freedom = 12
Weighted S.D. = 0.0004

All (except point) Mean = 0.9530, χ^2 = 56.1, Degrees of freedom = 19
Weighted S.D. = 0.0003

The probability of exceeding the χ^2 obtained is in each case <1%, and we must therefore conclude that the distribution contains errors other than those assumed (for example, positional errors, dead time correction errors). There is a barely significant difference between measurements in K09 and K13. If we scale up the

weighted standard deviations by the square root of (observed χ^2/degrees of freedom), that is we assume the additional errors have weight proportional to the known errors, we obtain

$$\bar{\phi}\ (\text{K09}) = 0.9516 \pm 0.0009$$
$$\bar{\phi}\ (\text{K13}) = 0.9541 \pm 0.0006$$
$$\bar{\phi}\ (\text{overall}) = 0.9530 \pm 0.0005$$

The corresponding figure for $\bar{\phi}$ (overall) for the ratios uncorrected for dead time is

$\bar{\phi}$ (overall, uncorrected) = 0.9551 ± 0.0005, thus the dead time correction, with an uncertainty of 33%, introduces an additional systematic error of 0.0007.

We conclude, therefore, that the mean of all measurements of the flux ratios in K09 and K13 relative to the centre, is

$$\bar{\phi} = 0.9530 \pm 0.0012$$

If we now assume that $\bar{\phi}$ is given by

$$\bar{\phi} = J_0 (24.13\ \beta) \quad \text{(i.e. Radius } r = 24.13 \text{ cm)}$$

$$\text{Then Var } \beta = \beta^2 \frac{\text{Var } r}{r^2} + \frac{\text{Var } \bar{\phi}}{r^2 J_1^2 (24.13\ \beta)}$$

Assuming a 1% uncertainty in r (i.e. r = 24.13 ± .24 cm)

$$\beta = 1.807 \pm 0.030\ \text{m}^{-2}$$

$$\beta^2 = 3.265 \pm 0.108\ \text{m}^{-2}$$

Appendix IV

Axial Scan Results

Table I

Cadmium Covered Results

(1) Counter position (cm)	(2) Axial chamber counts	(3) Monitor chamber counts	(4) Time for count (sec)	(5) (2)/(3) corrected for dead time	(6) $A\cos\frac{\pi(z-z_o)}{H}$	(7) (5)/(6)	χ^2 fitted points only
160	2166580	1.2×10^7	195	0.16666	0.17503	0.9522	-
155	2552478	"	"	0.19694	0.19935	0.9879	-
150	2876130	"	"	0.22248	0.22240	1.0004	0.02
145	3142050	"	"	0.24355	0.24321	1.0014	0.47
140	3372630	"	192	0.26160	0.26183	0.9991	-
135	3565998	"	"	0.27702	0.27816	0.9959	-
130	3733860	"	195	0.29078	0.29203	0.9957	-
125	3876000	"	"	0.30219	0.30233	0.9995	-
120	3995880	"	192	0.31150	0.31191	0.9987	0.61
115	8145000	2.4×10^7	384	0.31767	0.31772	0.9998	0.01
110	4100370	1.2×10^7	192	0.31991	0.32071	0.9975	2.24
105	4094019	"	"	0.31940	0.32081	0.9956	-
100	4055061	"	"	0.31626	0.31810	0.9942	-
95	3987540	"	"	0.31083	0.31258	0.9944	-
90	3892470	"	"	0.30318	0.30428	0.9964	-
85	3766062	"	195	0.29337	0.29331	1.0002	0.01
80	3605091	"	"	0.28047	0.27970	1.0028	2.26
75	-	-	-	-	-	-	-
70	3169209	1.2×10^7	195	0.24571	0.24518	1.0022	1.16
65	3863608	1.6×10^7	260	0.22419	0.22454	0.9984	-
60	2607000	1.2×10^7	195	0.20123	0.20195	0.9964	-
55	2300292	"	"	0.17713	0.17755	0.9976	-
50	1966731	"	"	0.15105	0.15161	0.9963	1.46

Table II

Bare Results

(1) Counter position (cm)	(2) Axial chamber counts	(3) Monitor chamber counts	(4) Time for count (sec)	(5) (2)/(3) corrected for dead time	(6) $A\cos\pi\frac{(z-z_o)}{H}$	(7) (5)/(6)	χ^2 fitted points only
160	3247520	2×10^6	148	1.64499	1.75892	0.9352	-
155	3890920	"	"	1.98427	2.00718	0.9886	-
150	4358420	"	"	2.23371	2.23732	0.9984	0.51
145	4767360	"	"	2.45393	2.44723	1.0027	1.67
140	5168320	"	"	2.67173	2.63501	1.0139	-
135	5525620	"	"	2.86739	2.79899	1.0244	-
130	5772640	"	"	3.00354	2.93768	1.0224	-
125	5894160	"	"	3.07078	3.04981	1.0069	-
120	6013540	"	"	3.13702	3.13440	1.0008	0.22
115	6083480	"	"	3.17590	3.19065	0.9954	6.86
110	6167660	"	"	3.22278	3.21806	1.0015	0.69
105	6210501	"	"	3.24667	3.21638	1.0094	-
100	6211740	"	"	3.24736	3.18564	1.0194	-
95	6128520	"	"	3.20097	3.12612	1.0239	-
90	5916680	"	"	3.08327	3.08340	1.0000	-
85	5645690	"	"	2.93348	2.92316	1.0035	3.53
80	5355300	"	"	2.77393	2.78151	0.9973	1.99
75	-	-	-	-	-	-	-
70	4719040	2×10^6	148	2.42781	2.42433	1.0014	0.45
65	-	-	-	-	-	-	-
60	3954380	2×10^6	148	2.01799	1.97961	1.0194	-
55	-	-	-	-	-	-	-
50	2896540	2×10^6	148	1.46183	1.46368	0.9987	0.16

For both bare and cadmium covered runs, the centre of the counter would have been level with the following positions at the following scale readings:-

Position	Scale Rdg. (cm)
Bottom of fuel	166.8
Top of 1st cluster	131.1
" " 2nd "	95.4
" " 3rd "	59.8
" " 4th "	24.1
Clean critical height	28.4

Appendix V

Manganese Foil Irradiations

Table I

Basic Results

Details of irradiation

Run No.:- I

Date:- 25.6.62

Diagram:- See Fig. 14

Axial foil positions:- 54.0 cms., 61.62 cms., 75.44 cms., 83.06 cms., (above bottom of fuel)

Results

Foil Posn.	Radius from cell centre (cm)	Radius from core centre (cm)	Foil No.	Activity (arbitrary) units	Foil calibration factor	Corrected activity (for each factor)	Macro-scopic correction factor	Final corrected activity x (normalised to centre) foil
54.0	0	17.062	-	-	-	-	-	-
"	1.322	15.740	45	133585	1.00004	133580	0.97955	0.33370
"	2.489	14.573	81	136014	0.98033	138743	0.98278	0.34546
"	3.658	13.404	74	149022	0.91186	163426	0.98542	0.40582
"	4.851	12.211	58	156562	0.96995	161412	0.98789	0.39982
"	6.020	11.042	78	189905	1.02848	184646	0.99008	0.45637
"	6.993	10.069	33	251629	1.00676	249930	0.99178	0.61666
"	7.938	9.124	52	245169	1.01387	241815	0.99323	0.59577
61.62	0	17.062	-	-	-	-	-	-
"	1.322	15.740	29	133773	1.00066	133645	0.99235	0.33407
"	2.489	14.573	47	138680	0.98370	140978	0.99563	0.35124
"	3.658	13.404	41	147785	1.00301	147342	0.99830	0.36612
"	4.851	12.211	44	161991	0.97013	166978	1.00080	0.41387
"	6.020	11.042	35	190996	0.98778	193359	1.00303	0.47820
"	6.993	10.069	31	233737	(uncal. 22.11.62)	233737	1.00473	0.57707
"	7.938	9.124	77	218721	"	218721	1.00622	0.53921
75.44	27.71	12.88	57	298978	0.98084	304635	0.96556	0.77204
"	12.55	8.62	22	337389	0.99674	338492	0.97285	0.85142
"	21.62	5.88	40	348758	0.99420	350793	0.97600	0.87952
"	18.98	2.58	10	367244	0.95080	386247	0.97822	0.96621
"	16.29	1.12	84	393566	0.98407	399937	0.97866	1.00000
83.06	27.71	12.88	60	270714	0.97185	278555	0.90045	0.76736
"	12.55	8.62	51	287651	0.94065	305800	0.90724	0.83613
"	21.62	5.88	56	328175	1.00377	326942	0.91017	0.89105
"	18.98	2.58	37	348556	0.97645	356962	0.91225	0.97066
"	16.29	1.12	32	361211	0.98177	367918	0.91265	1.00000

Table I

Basic Results (Cont'd)

Details of irradiation

Run No.:- II

Date:- 26.6.62

Diagram:- See Fig. 14

Axial foil positions:- 54.0 cms., 61.62 cms., 75.44 cms., 83.06 cms. (above bottom of fuel)

Results

Foil Posn.	Radius from cell centre (cm)	Radius from cell centre (cm)	Foil No.	Activity (arbitrary) units	Foil calibration factor	Corrected activity (for each factor)	Macro-scopic correction factor	Final corrected activity x (normalised to centre) foil
54.00	0	17.062	52	89031	1.01387	87813	0.97642	0.31606
"	1.322	15.740	78	93140	1.02848	905608	0.97955	0.32491
"	2.489	14.573	58	93121	0.96995	96006	0.98278	0.34331
"	3.658	13.404	74	-	0.91186	-	0.98542	-
"	4.851	12.211	81	112975	0.98033	115241	0.98789	0.40996
"	6.020	11.042	45	133797	1.00004	133792	0.99008	0.47491
"	6.993	10.069	33	176287	1.00676	175103	0.99178	0.62048
"	7.938	9.124	42	170510	(uncal. 22.11.62)	170510	0.99323	0.60332
61.62	0	17.062	-	-	-	-	-	-
"	1.322	15.740	35	92933	0.98778	94083	0.99235	0.33483
"	2.489	14.573	44	95510	0.97013	98451	0.99563	0.34922
"	3.658	13.404	41	103376	1.00301	103066	0.99830	0.36461
"	4.851	12.211	43	114401	0.98330	116297	1.00080	0.41039
"	6.020	11.042	29	132784	1.00066	132687	1.00303	0.46722
"	6.993	10.069	21	162867	(uncal. 22.11.62)	162867	1.00473	0.57248
"	7.938	9.124	37	153170	"	153170	1.00622	0.53760
75.44	27.71	12.88	57	206879	0.98084	210920	0.96556	0.76769
"	12.55	8.62	22	237789	0.99674	238567	0.97285	0.86179
"	21.62	5.88	40	243352	0.99420	244771	0.97600	0.88137
"	18.98	2.58	10	256160	0.95080	269415	0.97822	0.96791
"	16.29	1.12	84	274038	0.98407	278474	0.97866	1.00000
83.06	27.71	12.88	60	188295	0.97185	193740	0.90045	0.75987
"	12.55	8.62	51	204404	0.94065	217301	0.90724	0.84590
"	21.62	5.88	56	227326	1.00377	226472	0.91017	0.87875
"	18.98	2.58	57	242436	0.97645	248283	0.91225	0.96119
"	16.29	1.12	32	253711	0.98177	258422	0.91265	1.00000

Table II

Summary of Results

C_{i1} = Mean ratio of activity in run i to that in run 1 for each position measured.

$$\bar{C}_{21} = 1.01597 \qquad \bar{C}_{31} = 0.99468 \qquad \bar{C}_{41} = 1.01987$$

	Foil Posn.	Radius from cell centre (cm)	$x_1 \bar{C}_{11}$	$x_2 \bar{C}_{21}$	$x_3 \bar{C}_{31}$	$x_4 \bar{C}_{41}$	Mean	Standard deviation
	54.0	0	-	-	0.31435	-	0.31435	± .0135
In between	"	1.322	0.33370	0.33941	0.32315	0.34148	0.33444	± .0067
fuel	"	2.489	0.34546	0.35685	0.34145	0.35616	0.34998	± .0067
pellets	"	3.658	0.40583	0.37197	-	0.37185	0.38322	± .0078
	"	4.851	0.39982	0.42050	0.40774	0.41854	0.41165	± .0067
	"	6.020	0.45637	0.48484	0.47234	0.47650	0.47276	± .0067
Outside of pressure tube	"	6.993	0.61666	0.58629	0.61712	0.58386	0.60098	± .0121
Inside of cal. tube	"	7.938	0.59577	0.54782	0.60005	0.54828	0.57298	± .0121
	"	12.55	0.85142	0.84948	0.85712	0.86271	0.85518	± .0052
	"	16.29	1.00000	1.01597	0.99468	1.01987	1.00763	± .0052
Moderator	"	18.98	0.96621	0.98616	0.96266	0.98029	0.97383	± .0052
	"	21.62	0.87952	0.90528	0.87659	0.89621	0.88940	± .0052
	"	27.71	0.77204	0.77961	0.76353	0.77497	0.77254	± .0052

Remarks

1. The macroscopic correction factor includes a height correction to bring each foil position to 54.0 cms.

2. The standard deviations have been estimated from the average r.m.s. deviations of the individual results from their means, taking the fuel, pressure and calandria tubes, and moderator results as separate sets in computing the averages.

Appendix VI

Lu/Mn Results

Self-absorption correction to observed Lu/Mn ratio

[We are indebted to Mr. W. A. V. Brown for this section]

Consider an activated foil of finite thickness with its diameter large compared with its thickness, and assume that the γ sources are evenly distributed throughout the foil. When the γ-radiation from this foil is counted from one side only, some attenuation of the γ's by the material of the foil occurs. The transmission factor T, defined as the attenuated emission divided by the unattenuated emission, is given by:

$$T = \frac{F_2(o, x)}{x}$$

where $x = W\chi$

W is the foil thickness in gm/cm^2

χ is the γ mass absorption coefficient in cm^2/gm

$\chi = \mu/\rho$ where μ is the γ absorption coefficient (cm^{-1})
ρ is the foil density.

$$F_2(o, x) = \int_o^x E_2(t)\, dt$$

where $$E_2(t) = \int_t^\infty \frac{\exp(-y)\, dy}{y^2}$$

[Values of $F_n(b, x) = \int_o^x e^{bt} E_n(t)\, dt$ are tabulated by Van de Hulst in Astrophys Jnl. Vol. 107, No. 2, p.246 (1948).]

Assuming that the counting efficiency of the NaI crystal is constant for all radiation from a given element, and that 2π geometry is obtained, the mean transmission factor for the element will be the energy-dependent transmission factors weighted by the γ abundance at each energy. We have assumed that all radiation from manganese has the transmission factor appropriate to 0.82 MeV, since the largest effect is for the 113 and 208 KeV radiation from lutecium.

The following data was used:-

Element	γ Energy (MeV)	γ Abundance (%)	Mass absorption coeff'ts χ (cm^2/gm)		
			0.82 MeV	0.208 MeV	0.113 MeV
Mn	0.82	77	.065	.145	.300
	1.77	23			
Lu	0.113	31	.079	.660	2.350
	0.208	69			
Mg	-	-	.068	.120	.105
O	-	-	.070	.120	.145

The foils used contained the following proportions:-

Lu	4.1 ± 0.2	% by weight
Mn	6.0 ± 0.1	"
Mg	52.0	"
O	37.5	"

If we define $\left(\frac{Lu}{Mn}\right)_{\text{no absorption}} = \left(\frac{Lu}{Mn}\right)_{\text{observed}} \times F$

then $F = \frac{T_{Mn}}{T_{Lu}}$

The Table below gives values of F as a function of foil thickness (in gm/cm^2), and foil mass (for 0.42 inch diameter foils).

Foil thickness (gm/cm^2)	F	Mass of 0.42" dia. foil gm.
0	1	0
0.1	1.024	0.089
0.2	1.040	0.179
0.3	1.055	0.268
0.4	1.069	0.358
0.5	1.082	0.447
0.6	1.096	0.536
0.7	1.108	0.626
0.8	1.120	0.715
0.9	1.131	0.804
1.0	1.143	0.894
1.1	1.155	0.983

Table I

Basic Results

Run No.:- I

Date of irradiation:- 25.7.62

Time of start of irradiation:- 13 hrs. 13 mins. 37 secs.

Length of irradiation:- 45 mins.

Time of start of Mn counting:- 16 hrs. 48 mins. 25 secs. on 25.7.62

Time of start of Lu counting:- 9 hrs. 43 mins. on 27.7.62

Foil posn. height above bottom of fuel	Radius from cell centre (cms.)	Foil No.	Mass (gm)	Mn saturation activity	Lu saturation activity	Lu/Mn saturation activity	Mass correction factor	Corrected Lu/Mn	Lu/Mn in NESTOR	Ratio of core to NESTOR
54.0 cms.	0.80	D6	-	164743 ± 1827	261350 ± 12439	1.586 ± 0.078	1.0387	1.647 ± 0.081	1.304 ± 0.011	1.263 ± .063
"	1.95	D5	0.28678	355332 ± 3676	603157 ± 20085	1.697 ± 0.059	1.0572	1.794 ± 0.062	"	1.376 ± .047
"	3.15	D4	0.28971	378764 ± 3904	635293 ± 20791	1.677 ± 0.058	1.0578	1.774 ± 0.061	"	1.360 ± .047
"	4.30	D3	0.33888	465930 ± 4750	772281 ± 23883	1.658 ± 0.054	1.0655	1.767 ± 0.058	"	1.355 ± .046
"	5.45	D2	-	469495 ± 4786	756826 ± 23530	1.612 ± 0.053	1.0644	1.716 ± 0.056	"	1.316 ± .043

Time of start of Mn counting:- 18 hrs. 18 mins. 40 secs. on 25.7.62

Time of start of Lu counting:- 9 hrs. 42 mins. on 31.7.62

Foil posn.	Radius from cell centre (cms.)	Foil No.	Mass (gm)	Mn saturation activity	Lu saturation activity	Lu/Mn saturation activity	Mass correction factor	Corrected Lu/Mn	Lu/Mn in NESTOR	Ratio of core to NESTOR
75.5	12.59	D11	0.34220	1000142 ± 4080	1559210 ± 23605	1.559 ± 0.024	1.0661	1.662 ± 0.026	1.304 ± 0.011	1.275 ± .023
"	16.29	D10	0.31284	1097688 ± 4388	1692969 ± 24790	1.542 ± 0.023	1.0615	1.637 ± 0.024	"	1.255 ± .022
"	18.98	D9	-	1008748 ± 4101	1540169 ± 23435	1.527 ± 0.024	1.0644	1.625 ± 0.026	"	1.246 ± .023
"	27.71	D7	0.29236	784622 ± 3376	1232172 ± 20669	1.570 ± 0.027	1.0581	1.661 ± 0.029	"	1.274 ± .025

Table I

Basic Results (cont'd)

Run No.: II

Date of irradiation:- 26.7.62

Time of start of irradiation:- 13 hrs. 12 mins. 17 secs.

Length of irradiation:- 45 mins.

Time of start of Mn counting:- 14 hrs. 13 mins. 20 secs. on 26.7.62

Time of start of Lu counting:- 11 hrs. 18 mins. 6 secs. on 31.7.62

Foil posn. height above bottom of fuel	Radius from cell centre	Foil No.	Mass (gm)	Mn saturation activity	Lu saturation activity	Lu/Mn saturation activity	Mass correction factor	Corrected Lu/Mn	Lu/Mn in NESTOR	Ratio of core to NESTOR
54.0 cms	0.80	D14	-	201461 ± 4125	394026 ± 12040	1.956 ± 0.072	1.0387	2.032 ± 0.075	1.304 ± 0.011	1.558 ± .059
"	1.95	D17	0.33592	323925 ± 6565	700341 ± 15212	2.162 ± 0.064	1.0648	2.302 ± 0.068	"	1.765 ± .054
"	3.15	D15	0.36229	376146 ± 7613	794553 ± 15950	2.112 ± 0.060	1.0693	2.258 ± 0.064	"	1.732 ± .051
"	4.30	D18	0.34901	385023 ± 7787	810048 ± 16330	2.104 ± 0.060	1.0663	2.243 ± 0.064	"	1.720 ± .052
"	5.45	D16	0.37516	466307 ± 9410	949577 ± 17739	2.036 ± 0.056	1.0713	2.181 ± 0.060	"	1.673 ± .048
* 58.60	102.4	D12	0.31264	696119 ± 13996	1179402 ± 20078	1.694 ± 0.045	1.0615	1.798 ± 0.048	"	1.379 ± .039

*Measurement in K19 search tube (i.e. in D_2O reflector)

Table II

Results of Foil Calibrations in the NESTOR Thermal Column

Run No.:	I	II
Date of irradiation:	29.8.62	June 1962
Time of start of irradiation:	9 hrs. 18 mins.	Refer - SGHW II
Length of irradiation:	4 hrs.	NESTOR calibrations
Time of start Mn counting:	19 hrs. 38 m. 13 s. on 29.8.62	
Time of start Lu counting:	10 hrs. 16 m. 45 s. on 31.8.62	

Run No.	Foil No.	Mass (gm)	Mn saturation activity	Lu saturation activity	Lu/Mn saturation activity	Mean mass correction factor	Corrected Lu/Mn	Mean corrected ratio for 0.4215" dia. foils
I	D29	0.33113	310841	375651	1.208 ± .029		1.281 ± .031	1.304 ± .011
"	D34	0.33113	330015	390484	1.183 ± .028	1.06037	1.254 ± .030	
"	D35	0.33182	335941	398502	1.184 ± .028		1.255 ± .030	
II				Refer to	1.222 ± .029		1.296 ± .031	
"				SGHW II	1.233 ± .029		1.307 ± .031	
"				NESTOR	1.223 ± .029	1.06037	1.297 ± .031	
"				calibrations	1.317 ± .029		1.397 ± .031	
"					1.265 ± .029		1.341 ± .031	

Table III

Summary of results of Lu/Mn ratio

Lu/Mn Ratio Relative to NESTOR Thermal Column

Foil Posn.	Radius from cell centre	Run No.		Remarks
		I	II	
In between fuel pencils	0.80	1.263 ± 0.063	1.558 ± 0.059	No mean is quoted due to the inconsistency of the results
	1.95	1.376 ± 0.047	1.765 ± 0.054	
	3.15	1.360 ± 0.047	1.732 ± 0.051	
	4.30	1.355 ± 0.046	1.720 ± 0.052	
	5.45	1.316 ± 0.043	1.673 ± 0.048	
On DIMPLE foil machine in moderator	12.55	1.275 ± 0.023		
	16.29	1.255 ± 0.022		
	18.98	1.246 ± 0.023		
	27.71	1.247 ± 0.025		
In D_2O reflector (K19)			1.379 ± 0.039	

Manganese/Lutecium foil irradiation

Table IV

Basic Results from the Manganese Activity

Run No.	I	II
Date of irradiation	25-7-62	26-7-62
Axial foil positions	54.0 cms., 75.5 cms.	54.0 cms.

Run No.	Foil Position above bottom of fuel (cms.)	Radius from cell centre (cms.)	Radius from core centre (cms.)	Foil No.	Mass (gms.)	Mn Saturation Activity	mass corrected	macro-scopic correction factor	Final corrected activity x normalised to foil at 1.95 cms. P.C.R.
I	54.0	0.8	16.26	D6	0.17188*	164743	958477	0.96284	0.77586
"	"	1.95	15.11	D5	0.28678	355332	1239040	0.96570	1.00000
"	"	3.15	13.91	D4	0.28971	378764	1307390	0.96848	1.05214
"	"	4.30	12.76	D3	0.33888	465930	1374911	0.97092	1.10369
"	"	5.45	11.61	D2	0.33113‡	469495	1417857	0.97315	1.13556
"	75.5	12.55	8.62	D11	0.34220	1000142	2922683	0.95720	2.84003
"	"	16.29	1.12	D10	0.31284	1097688	3508784	0.96292	2.84003
"	"	18.98	2.58	D9	0.33113‡	1008748	3046381	0.76249	2.46686
"	"	27.71	12.88	D7	0.29236	784622	2683753	0.95069	2.20011
II	54.0	0.80	16.26	D14	0.17188*	201461	1172103	0.96284	1.21912
"	"	1.95	15.11	D17	0.33592	323925	964292	0.96570	1.00000
"	"	3.15	13.91	D15	0.36229	376146	1038246	0.96848	1.07360
"	"	4.30	13.76	D18	0.34901	385023	1103186	0.97092	1.13789
"	"	5.45	11.61	D16	0.37516	466307	1242955	0.97315	1.27911

Remarks

* As these specially shaped foils are unweighed, a mean figure for the foils in this fuel position is used.

‡ Also unweighed foils. The mean mass used is obtained from the masses of all the 0.4212" dia., foils.

A Height correction is included in the macroscopic correction factor.

Table V

Summary of Results

Mn Activity from Lu/Mn

C_{21} = Mean ratio of activity in run 2 to that in run 1 for each position measured.

$\bar{C}_{21}$ = 0.95943

Foil Posn.	Radius from cell centre (cm)	$x_1 \bar{C}_{11}$	$x_2 \bar{C}_{21}$	Mean	Standard deviation
54.0	0.8	0.77586	1.16966	0.97276	0.19690
"	1.95	1.00000	0.95943	0.97972	0.01545
"	3.15	1.05214	1.03004	1.04109	0.01545
"	4.30	1.10369	1.09173	1.09771	0.01545
"	5.45	1.13556	1.22722	1.18139	0.04583
"	12.55	2.37978	-	2.37978	0.02185
"	16.29	2.84003	-	2.84003	0.02185
"	18.98	2.46686	-	2.46686	*
"	27.71	2.20011	-	2.20011	0.02185

*Error uncertain since foil was unweighted. A 13% spread in foil masses indicates the uncertainty to be of order ± 5%.

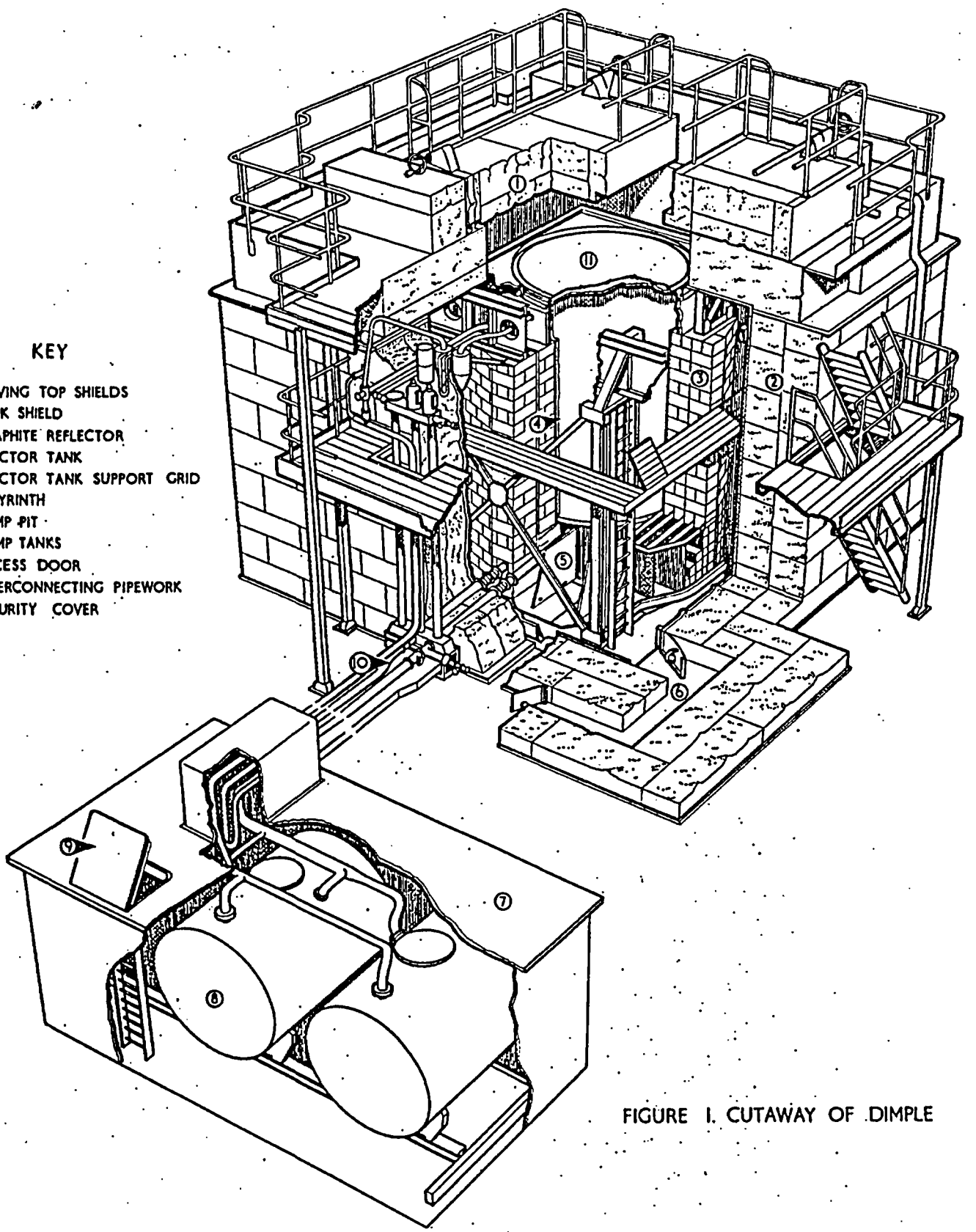

FIGURE 1. CUTAWAY OF DIMPLE

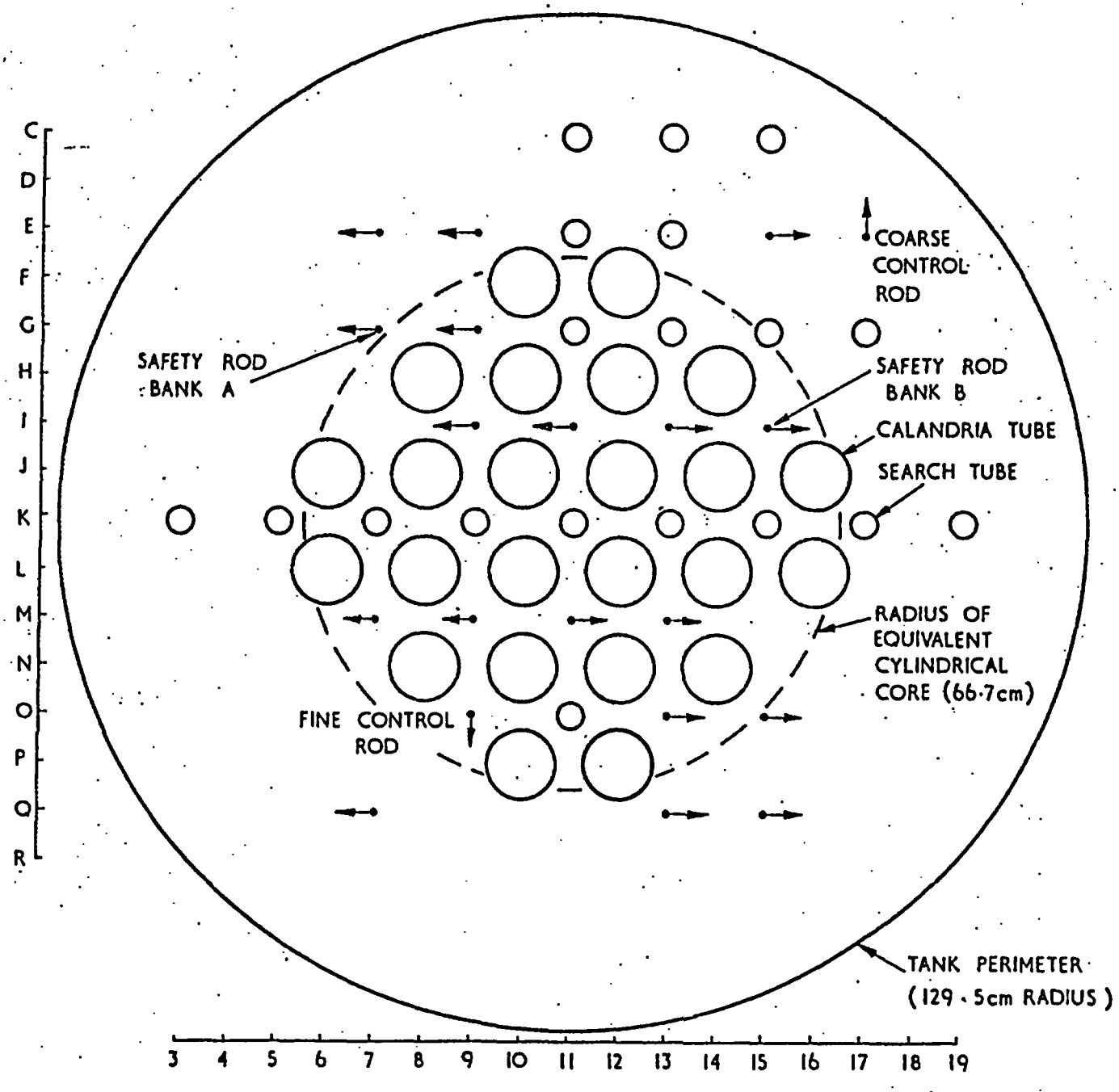

FIG. 2 PLAN VIEW OF REACTOR TANK SHOWING FUEL, SEARCH TUBES, SAFETY AND CONTROL RODS.

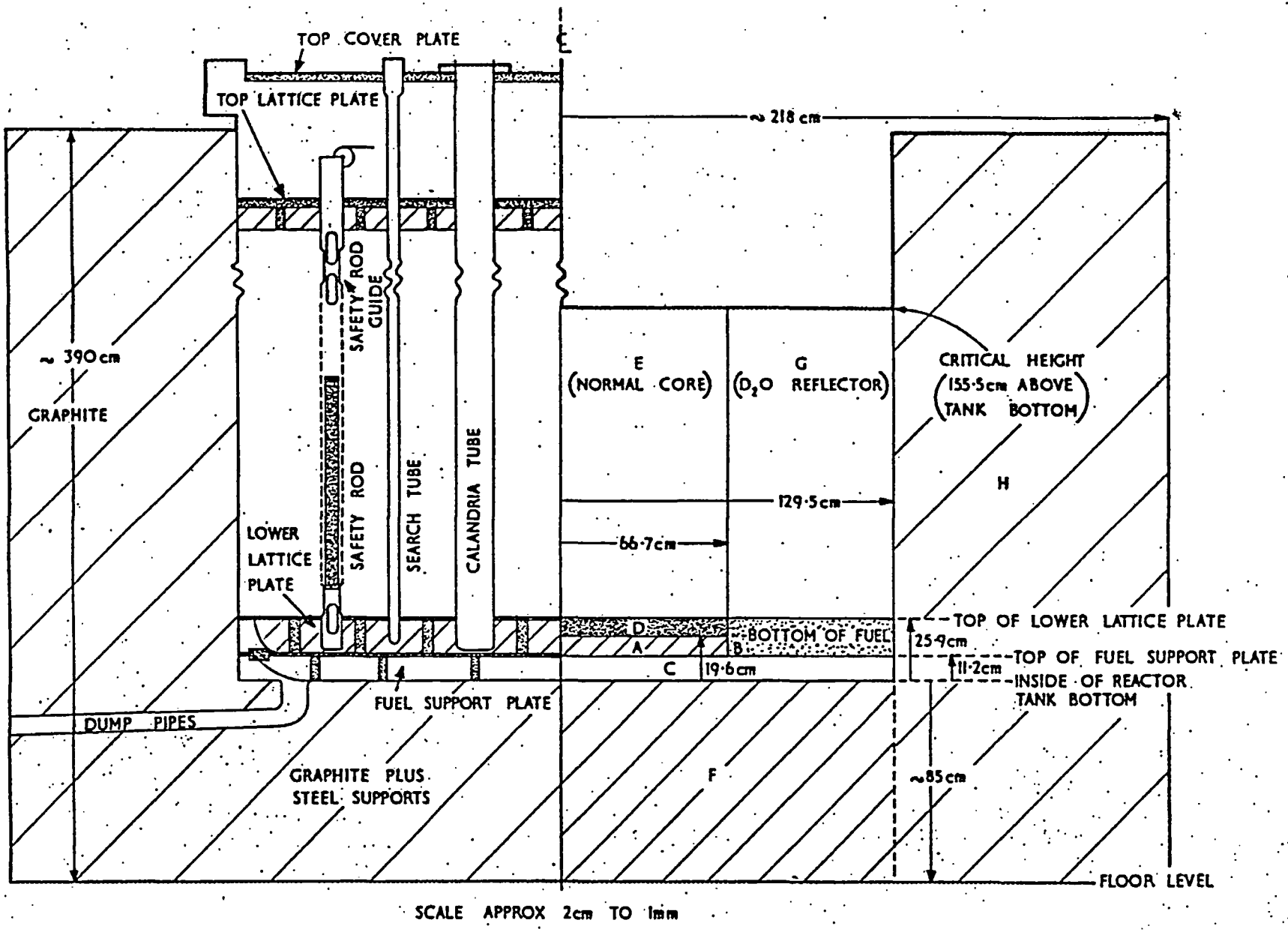

FIG. 3(a) SECTION THROUGH REACTOR

FIG.3(b) SIMPLIFIED SECTION THROUGH REACTOR GIVING REGIONS OF DIFFERENT PHYSICAL PROPERTIES

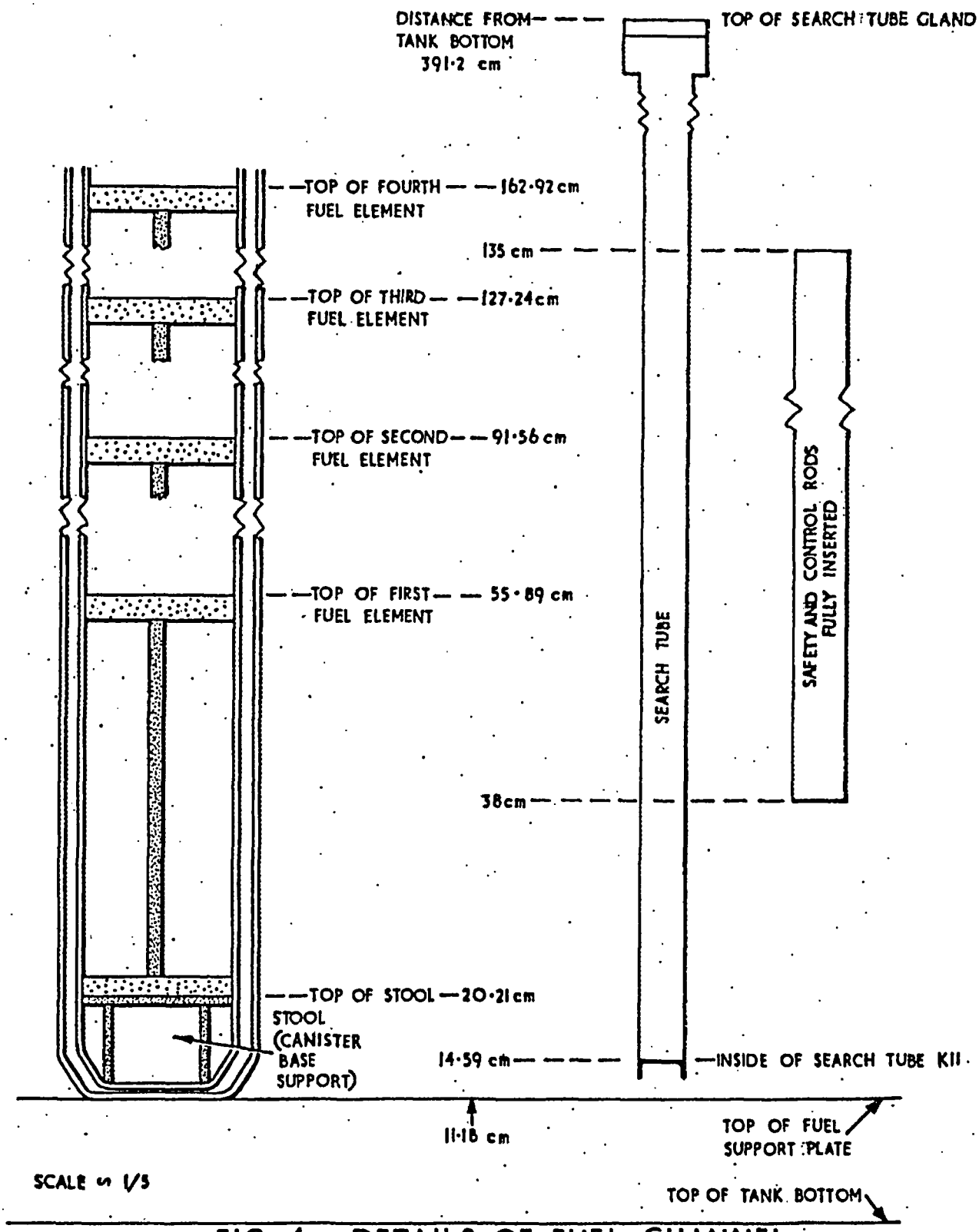

FIG. 4 DETAILS OF FUEL CHANNEL, SEARCH TUBES AND SAFETY RODS

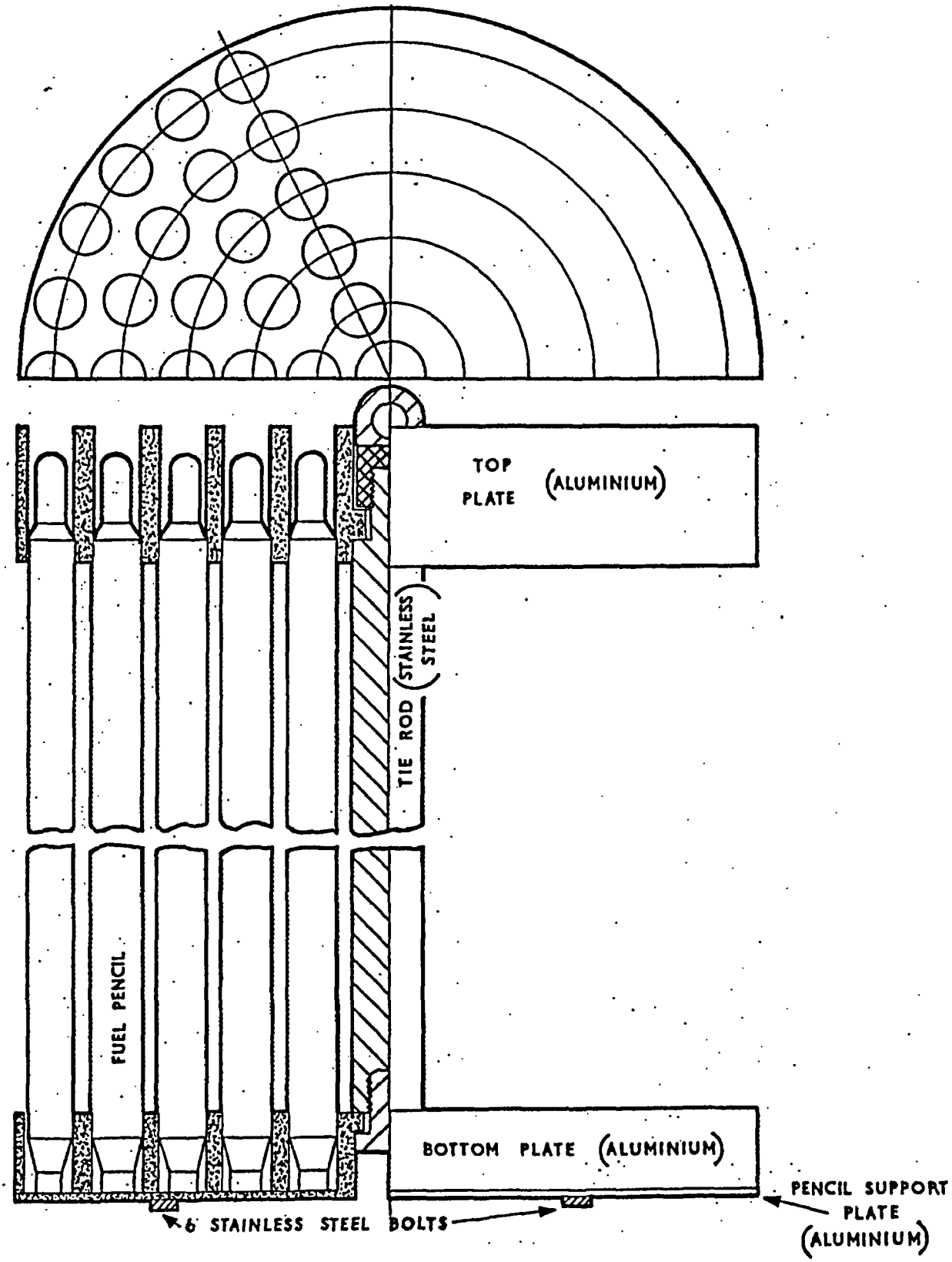

FIG. 5 DIAGRAM OF FUEL CLUSTER

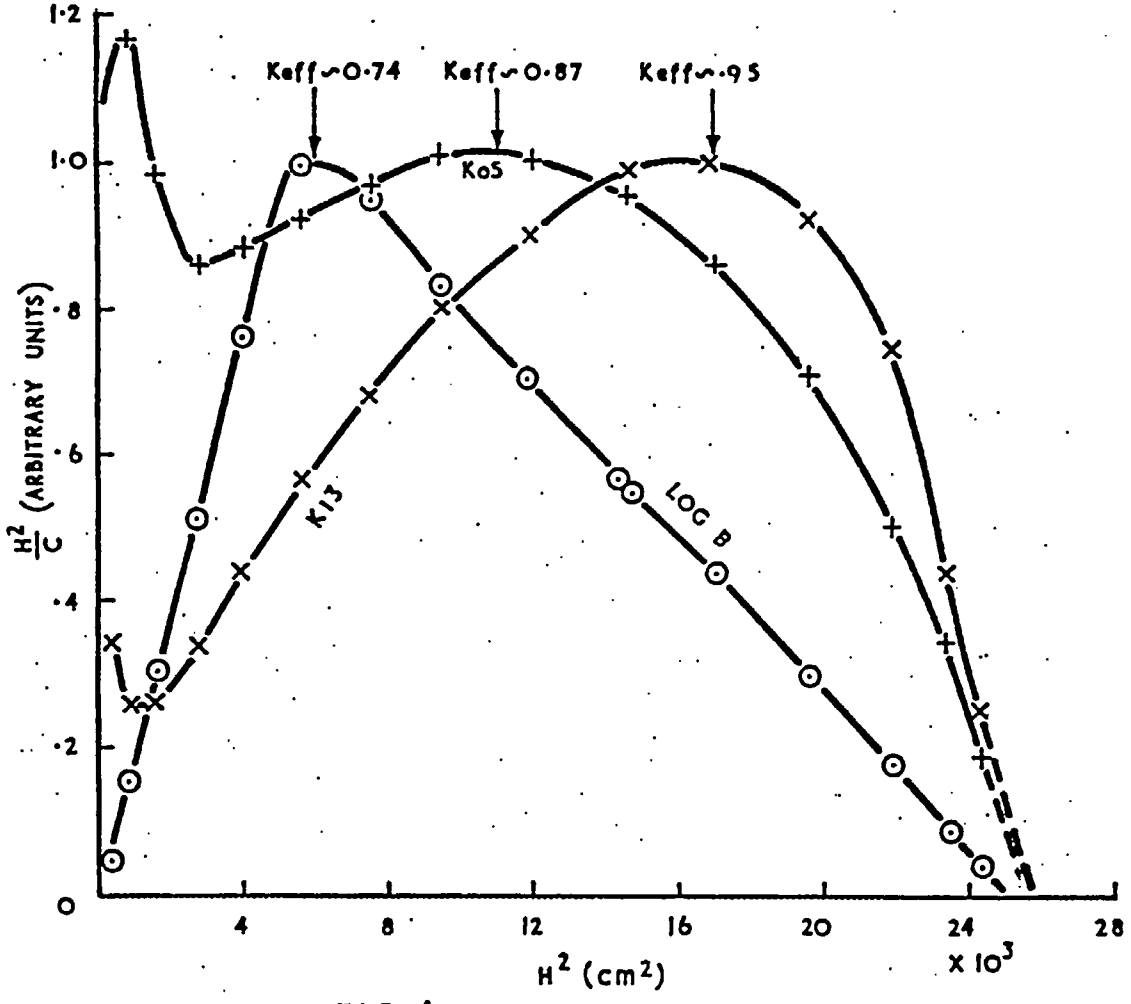

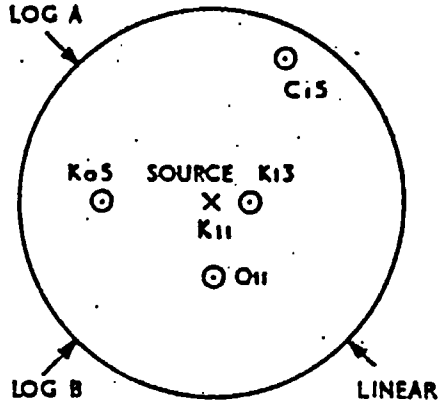

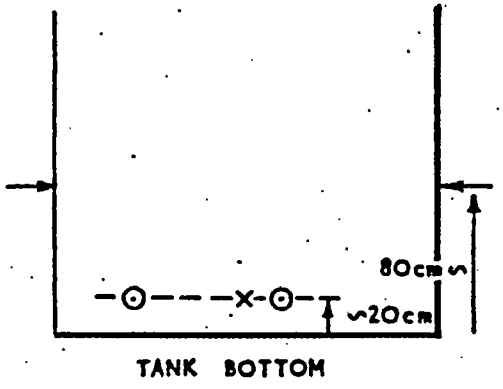

FIG 6. MODERATOR APPROACH-TO-CRITICAL CURVES

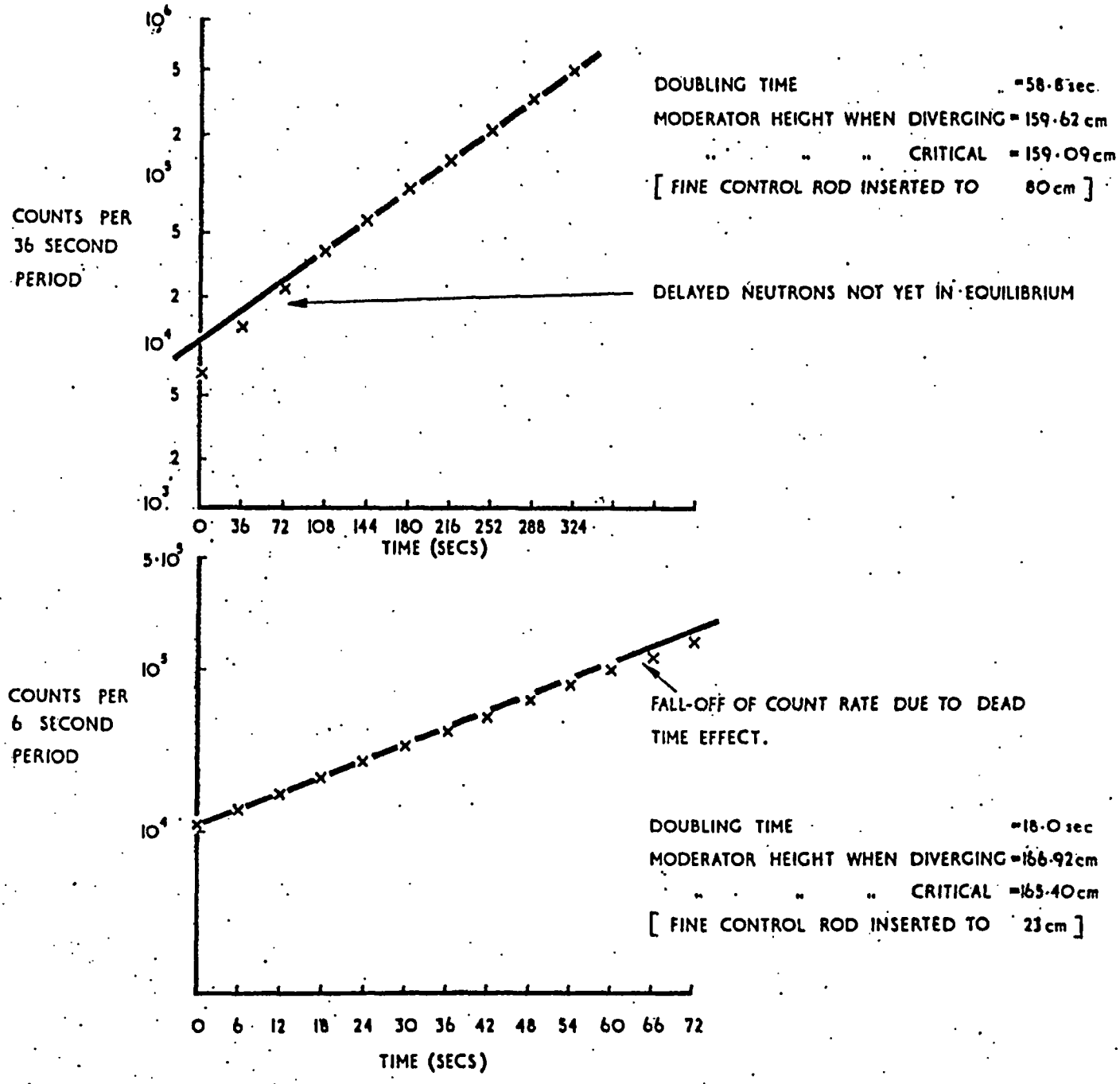

FIG. 7 EXAMPLES OF MEASUREMENT OF SLOW AND FAST DOUBLING TIMES

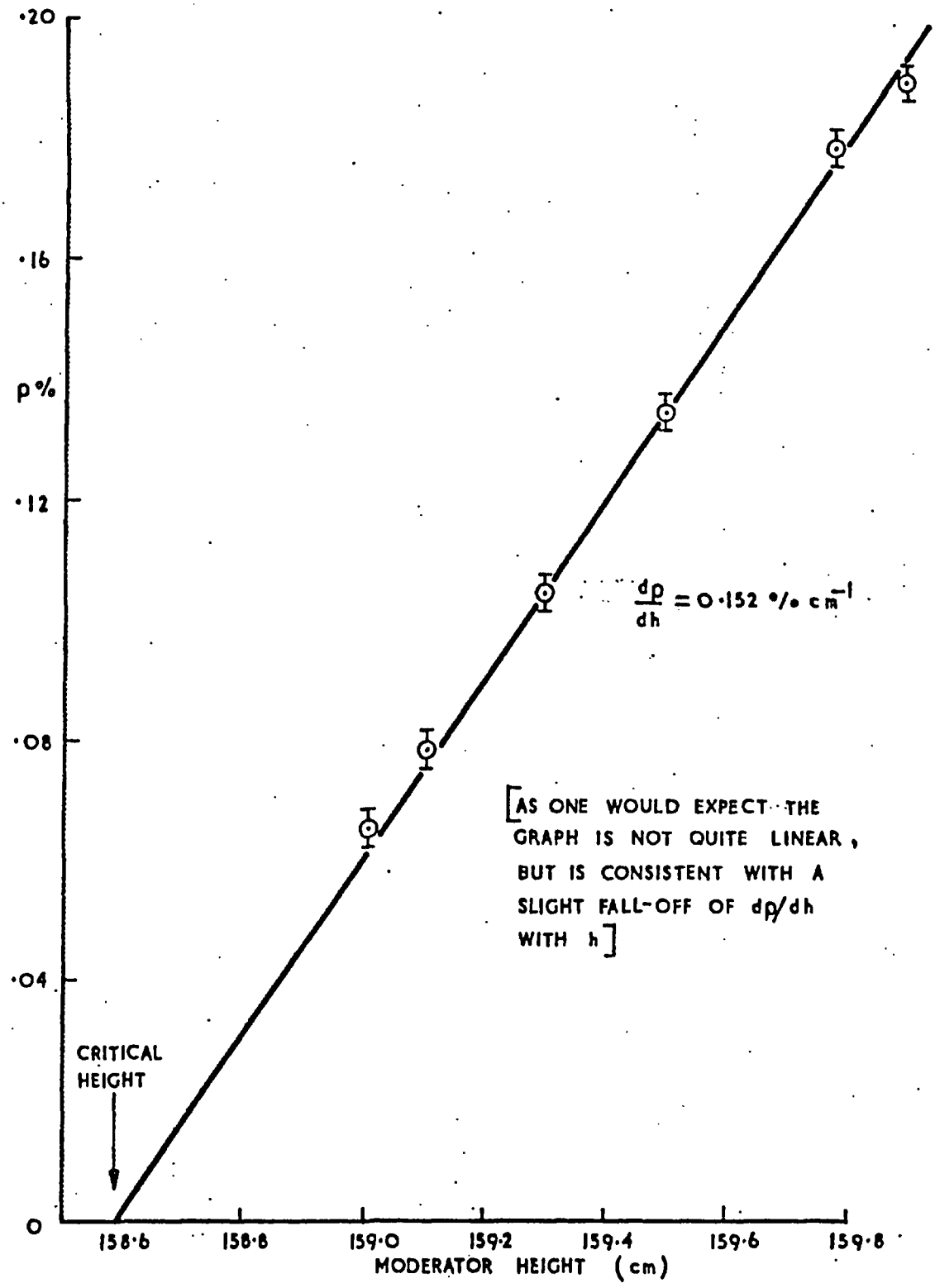

FIG 8. A TYPICAL REACTIVITY VERSUS HEIGHT GRAPH.

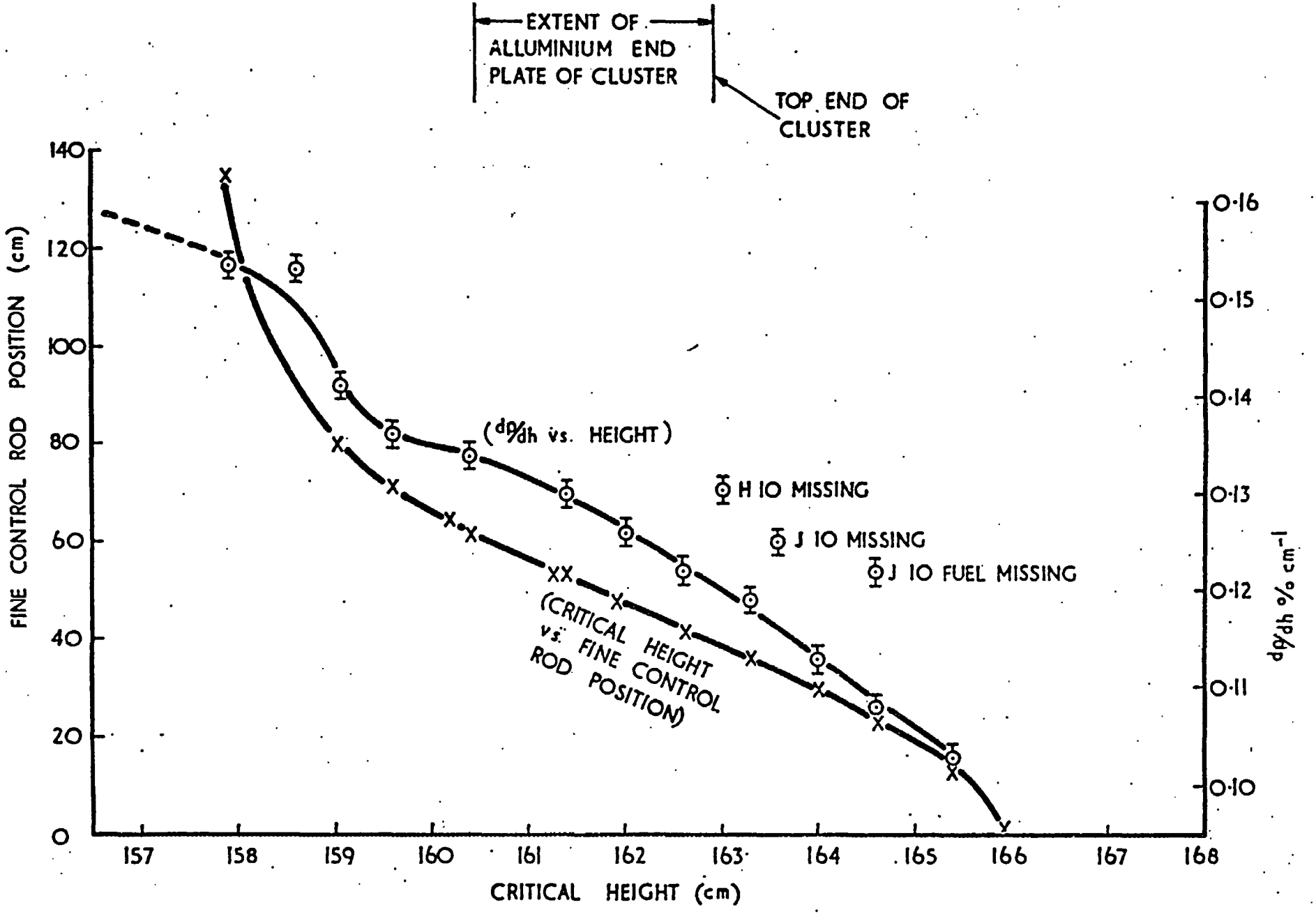

FIG 9. $\frac{dp}{dh}$ AND FINE-CONTROL ROD POSITION VS CRITICAL MODERATOR HEIGH

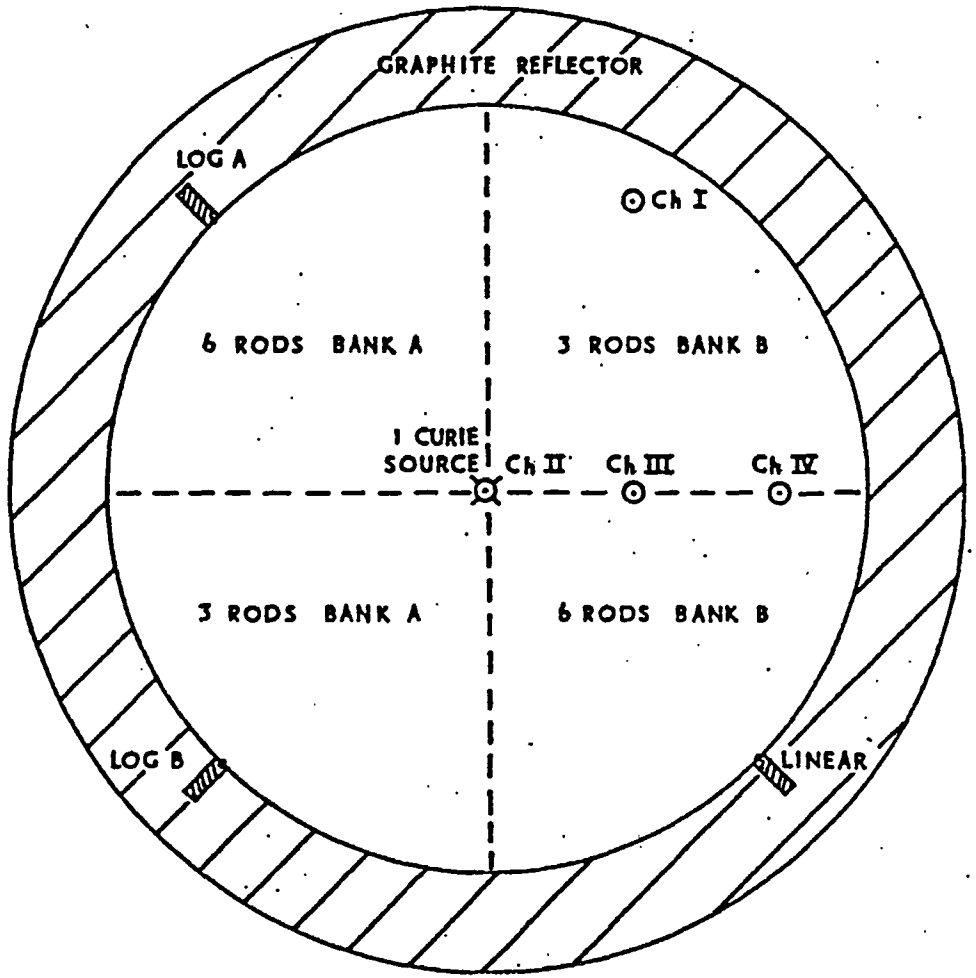

AXIAL POS'NS
SOURCE ABOUT 16 cm ABOVE TANK BOTTOM
ALL BF_3 COUNTERS ABOUT 80 cm ABOVE TANK BOTTOM

FIG 10:SOURCE AND DETECTOR POSITIONS FOR SUBCRITICAL REACTIVITY MEASUREMENTS

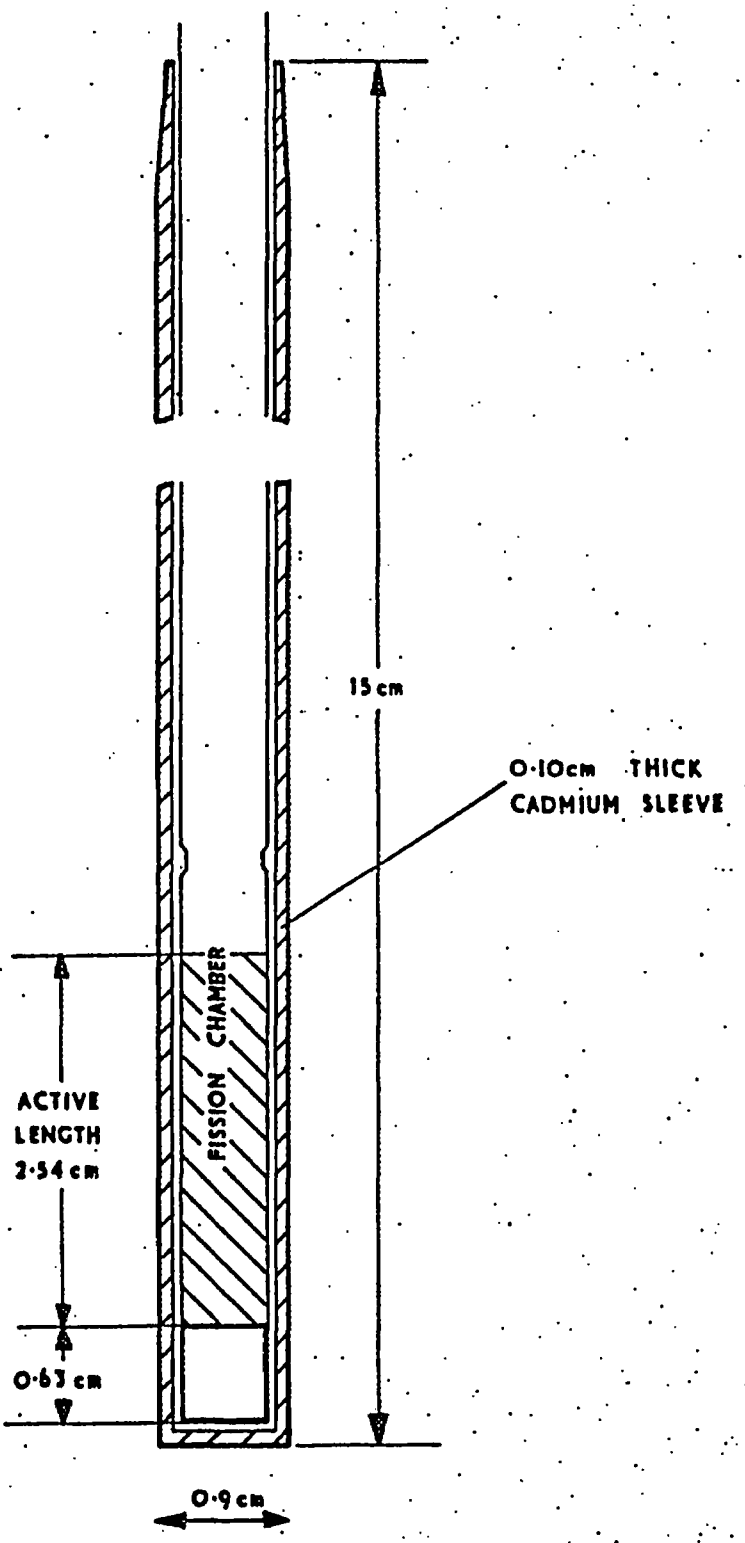

FIG. 11 DIAGRAM OF FISSION CHAMBER WITH CADMIUM SLEEVE

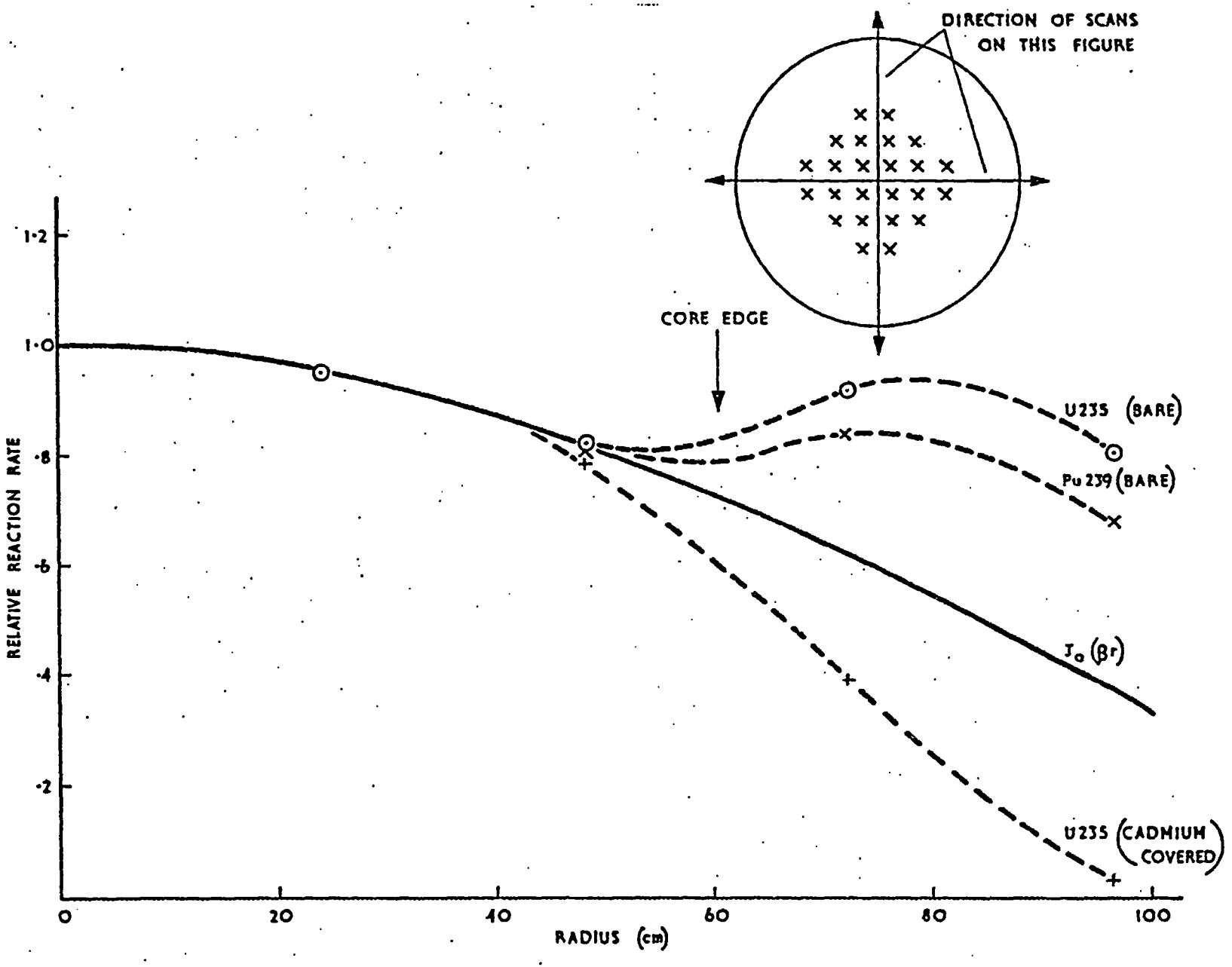

FIG. 12 RADIAL REACTION RATES IN SEARCH TUBES THROUGH MAJOR AXES

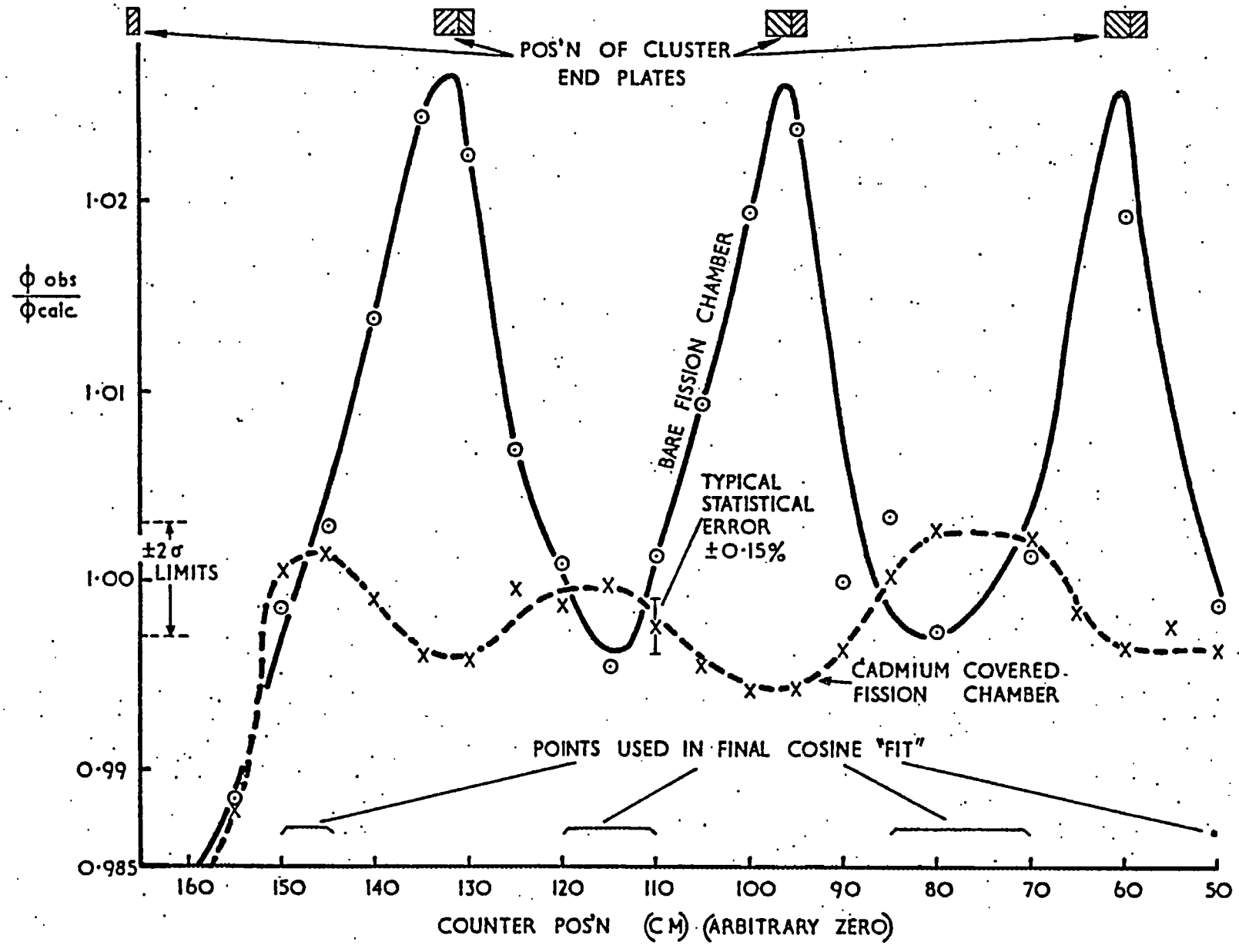

FIG. 13 EXPERIMENTAL AXIAL U235 REACTION RATE DISTRIBUTION IN K II DIVIDED BY FITTED COSINE

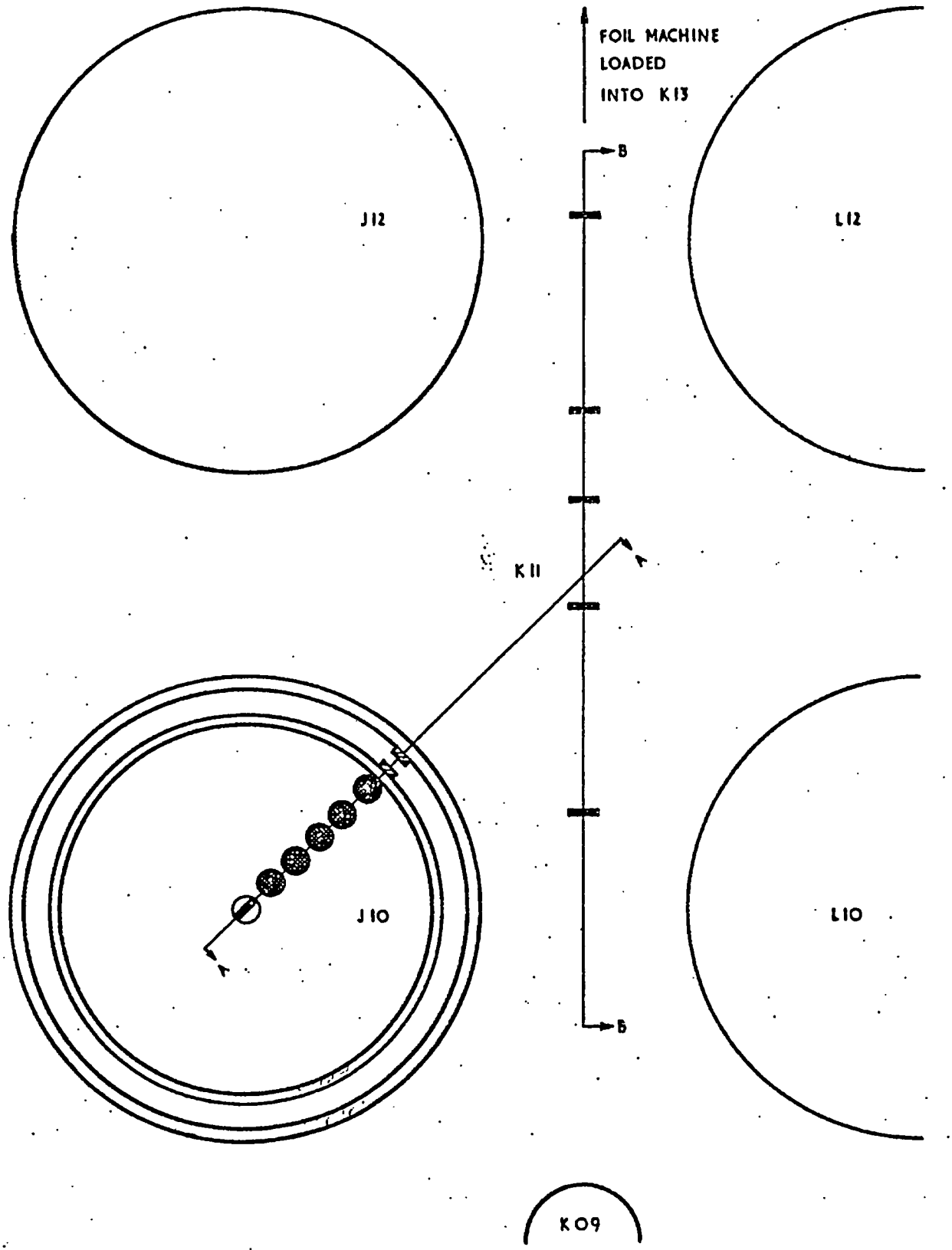

FIG.14 ARRANGEMENT FOR LATTICE CELL FOIL IRRADIATIONS

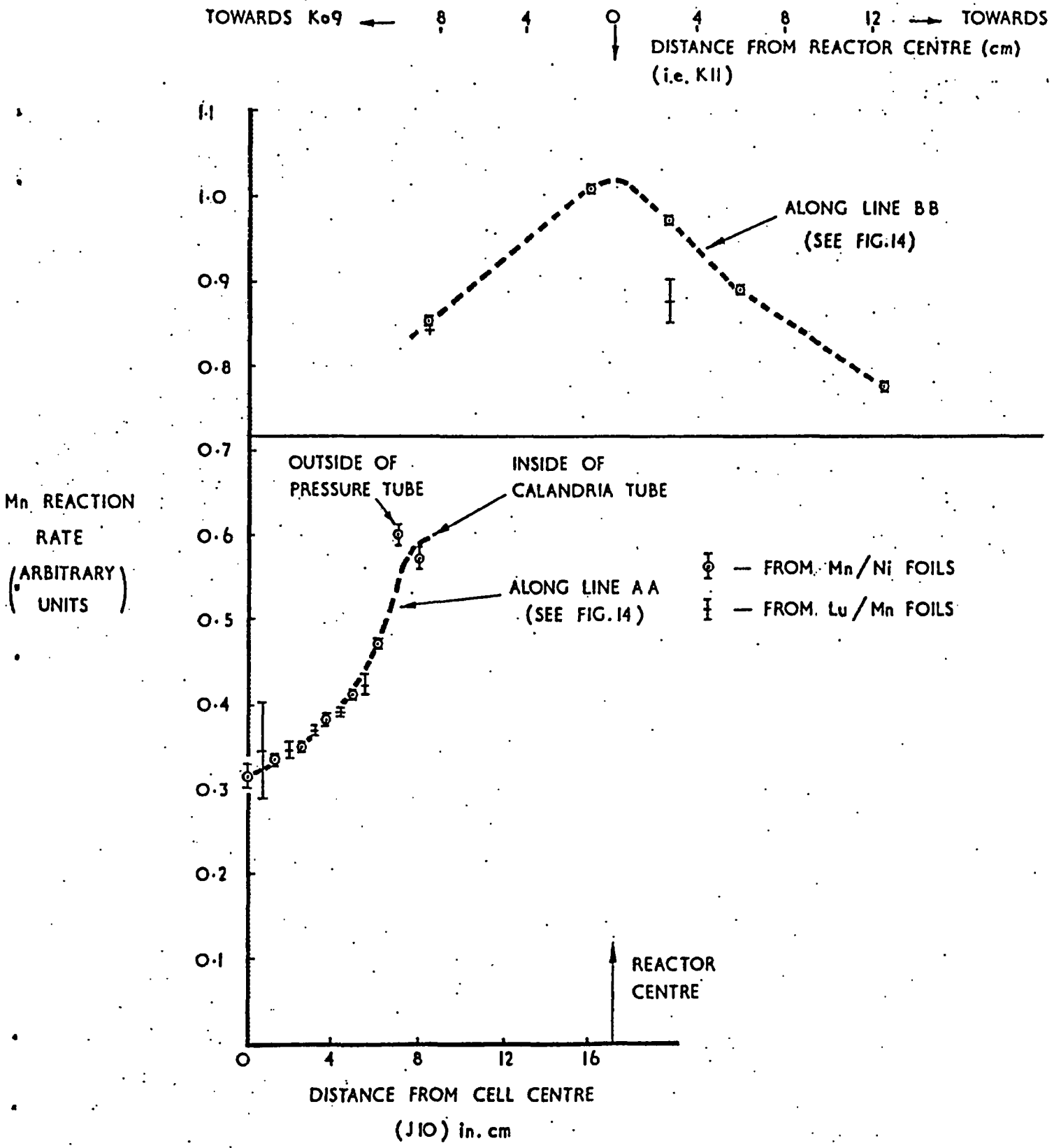

FIG. 15 MANGANESE REACTION RATES IN THE LATTICE CELL

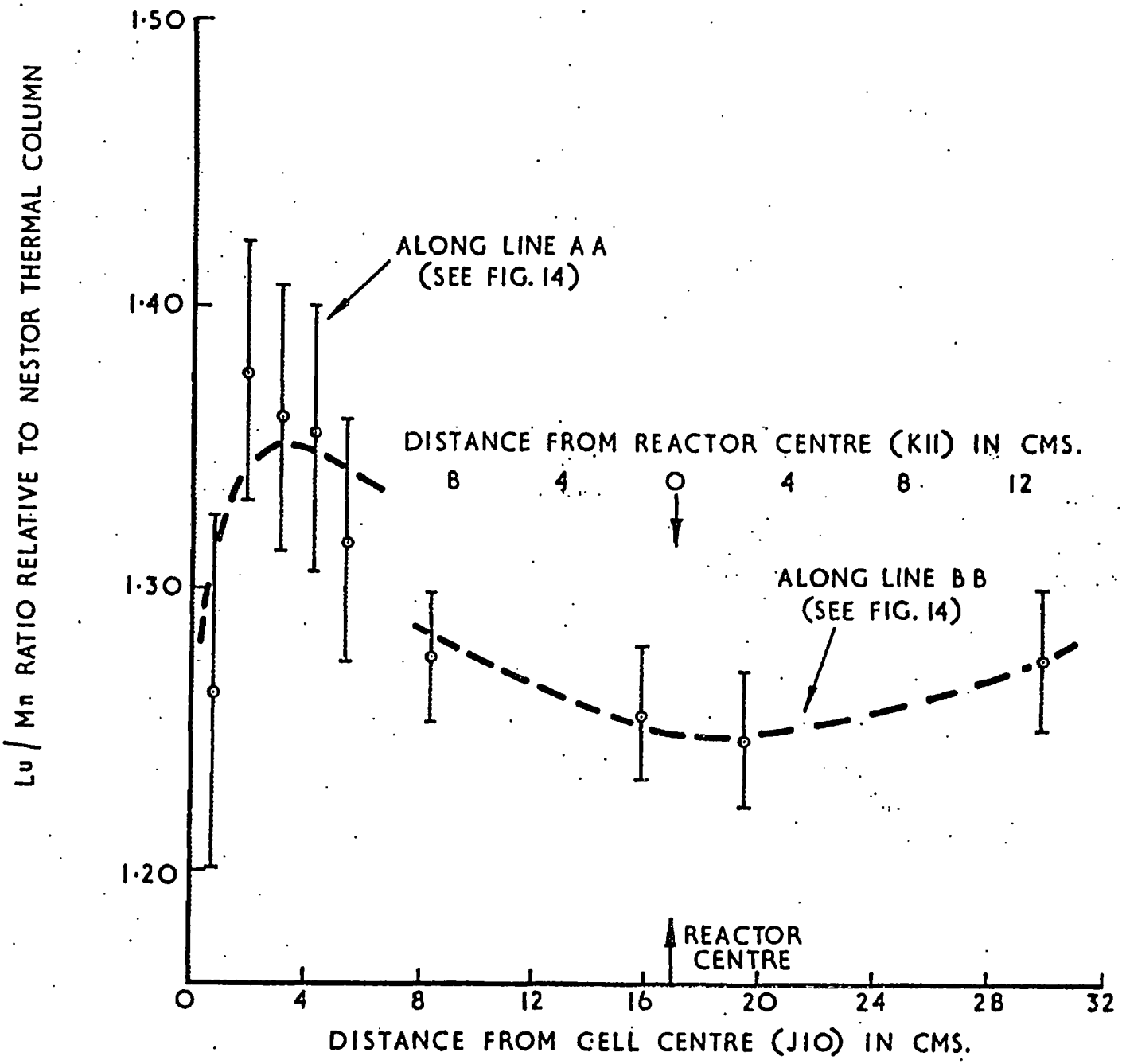

FIG.16 Lu/Mn RATIOS - FIRST IRRADIATION ONLY